The influence of heat treatment on the phase relations in mineral growth systems

Dissertation
zur Erlangung des Grades
„Doktor der Naturwissenschafter“

am Fachbereich Chemie, Pharmazie und Geowissenschaften
der Johannes Gutenberg-Universität Mainz

Bhuwadol Wanthanachaisaeng
geb. in Chonburi, Thailand

Mainz, 2007

Tag der mündlichen Prüfung:

ZUSAMMENFASSUNG

Die Farbvarietäten von Korund (gelbe, blaue und grüne Saphire, Rubin und Padparadscha) gehören zu den bekanntesten Farbedelsteinen. Sie werden im kommerziellen Bereich häufig einer Temperaturbehandlung unterzogen, um sie farblich zu verbessern. Auch wenn dieses Verfahren im Edelsteinhandel akzeptiert ist, ist insbesondere bei wertvolleren Steinen ein Preisunterschied zwischen behandelten und unbehandelten Steinen festzustellen. Der Nachweis einer Temperaturbehandlung erfolgt über die Veränderung des Einschlussbildes. In der vorliegenden Arbeit wurde insbesondere die Veränderung von Aluminiumhydroxiden und die Kristallinität von Zirkon und dessen Phasenumwandlung untersucht.

Aluminiumhydroxideinschlüsse wurden mit der DTA und TG untersucht und die Diagramme mit denen von Diaspor, Boehmit, Gibbsit und Bayerit verglichen.

Zirkon-Einschlüsse in chromhaltigen Korunden von Ilakaka (Madagaskar) wurden vor einer Temperaturbehandlung auf ihre Strahlungsschäden mit Hilfe der Raman-Spektroskopie und Umgebungsdrücke mit Hilfe des Cr^{3+} Fluoreszenz-shifts untersucht. Anschließend wurden die gleichen Steine einer Temperaturbehandlungen bei 500, 800, 1000, 1200, 1400, 1600 und 1800°C unterzogen, je 3 Stunden bei jeder Stufe getempert und nach jeder Stufe charakterisiert. Nach der Behandlung bei 1000°C zeigt die □$_3$ Raman-Bande der Zirkone die geringste Halbwertsbreite, die niedrigste Raman-Bandenverschiebung und den niedrigsten Umgebungsdruck. Somit ist eine Hitzebehandlung unter den verwendeten Bedingungen bereits sicher ab 1000°C Raman-spektroskopisch nachweisbar. Mikroskopisch verändern sich die Einschlüsse erst ab 1400°C, sie zeigen dann eine weißliche Oberfläche. Diese „frostige“ Oberfläche zeigt die Zersetzung des Zirkons in m-ZrO_2 und einem SiO_2-haltiges Glas an, die bereits ab 1200°C Raman-spektroskopisch nachweisbar ist. In Verbindung mit der Zersetzung des Zirkons, steigt der Umgebungsdruck um den Einschluss und die Raman-Bandenverschiebung des ν_3-Peaks. Nach der Behandlung bei 1800°C kann man nur noch ehemals geschmolzene Einschlüsse erkennen, sie sind komplett in m-ZrO_2 und ein SiO_2-haltiges Glas umgewandelt worden.

ABSTRACT

Corundum is one of the most famous gems materials. Different heat treatment methods for enhancement purposes are commonly applied and accepted in the gem market. With this reason, the identification of the natural, unheated corundum is intensively investigated. In this study, aluminium hydroxide minerals and zircon are focused to observe the crystallization and phase change of these minerals during heat treatment procedures.

Aluminium hydroxide minerals can be transformed to alumina with the corundum structure by heating. The reaction history of aluminium hydroxide minerals containing corundum was investigated comparing it with diaspore, boehmite, gibbsite and bayerite by TG and DTA methods. These hydroxide minerals were entirely transformed to corundum after heating at 600°C.

Zircon inclusions in corundums from Ilakaka, Madagascar, were investigated for the influence of different heat-treatment temperatures on the recovery of their crystalline structure and on possible reactions within and with the host crystals. The host corundum was heated at 500, 800, 1000, 1200, 1400, 1600 and 1800°C. The crystallinity, the trapped pressure, and the decomposition of the zircon inclusions within the host corundum have been investigated by Raman spectroscopy. Radiation-damaged zircon inclusions may be used as an indicator for unheated Ilakaka corundum crystals. They are fully recrystallized after heating at 1000°C influencing the lowering of the ν_3 Raman band shift, the decreasing of FWHM of the ν_3 Raman band and the decreasing of the trapped pressure between the inclusion and the host corundum. Under microscopic observation, surface alterations of the inclusions can be firstly seen from transparent into frosted-like appearance at 1400°C. Then, between 1600°C and 1800 °C, the inclusion becomes partly or even completely molten. The decomposition of the zircon inclusion to m-ZrO_2 and SiO_2-glass phases begins at the rim of the inclusion after heating from 1200°C to 1600°C which can be detected by the surface change, the increase of the ν_3 Raman band position and the trapped pressure. At 1800°C, the zircon inclusions entirely melt transforming to solid phases during cooling like m-ZrO_2 and SiO_2-glass accompanied by an increase of pressure between the transformed inclusion and its host.

TABLE OF CONTENTS

1. Introduction

1.1 Corundum

Corundum (α-Al_2O_3) is an oxide mineral in the hematite group with the ratio of metal to oxygen as X_2O_3. The crystal symmetry is trigonal ($R\bar{3}c$). The structure is based on octahedral coordination of Al^{3+} cations by O^{2-} anions according to the hexagonal close packing. In the structure, there are 1/3 of the octahedral sides vacant, 2/3 are occupied by Al^{3+} cations. One octahedral void shares 3 edges and 1 face with other octahedral sites (Fig. 1.1). The ionic radius of Al^{3+} is 0.535Å (Shannon, 1976). Other cations, that have similar radii with Al^{3+}, can substitute aluminium such as Fe^{3+} (0.55 Å) and Cr^{3+} (0.615 Å). There are also other trace elements in the octahedral sites such as Ti (0.74 Å), V (0.59 Å), Mg (0.72 Å) and Fe^{2+} (0.69 Å) and others which would be a cause of colours of corundum. Smaller trace elements like Be and H could occupy the tetrahedral sites.

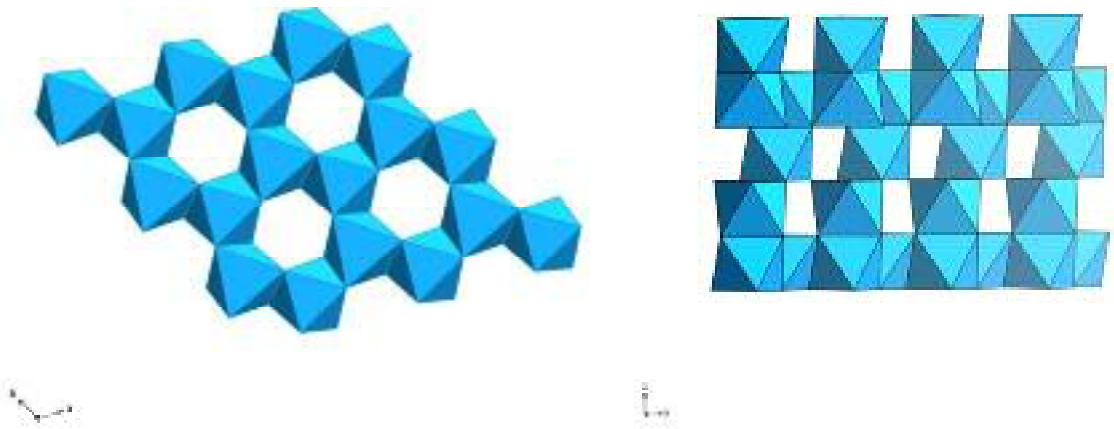

Fig. 1.1 Corundum (α-Al_2O_3) structure showing one octahedron vacant for every two octahedrally occupied voids.

1.2 Heated corundum

Corundum species are among the most famous and precious gem materials. For a long time, it has been highly demanded in the gems and jewellery business mainly because of its hardness and its variety in colour. The hardness of corundum is 9 in the Mohs scale (where the hardest is diamond, 10), which is one good reason to be set up as a jewellery material. Besides, there are many varieties of corundum, categorized by its colour, such as ruby for red corundum, blue sapphire for the blue one, Padparadcha (mixture of pinkish orange to orangey pink with the pastel tones and low to medium saturations; Laboratory Manual Harmonisation Committee (LMHC), 2006), and fancy sapphire for the other colours like yellow, green etc.. Therefore, new corundum sources as well as the propagation of enhancement investigations are always required to supply the gem market.

A naturally provided overall good quality corundum is, normally, very rare. However, there are many methods to improve the colour and clarity such as heat treatment, irradiation, and so forth. The heat treatment method is commonly applied and accepted in the gem market, but the heated corundum affects the market price, for it is beautiful like the untreated one with good quality but with the cheaper price. With this reason, the identification of the unheated corundum is necessary for both buyers and sellers. The gemmologists have been trying to study and improve the identification methods diversely. They found some classical changing evidences in the heat-treated corundum, for instance, the dissolution of rutile needle (resorbed needles) inclusions, which can be seen after any high temperature-heating process. It is an important indicator identifying heated corundums (e.g. Hänni, 1982; Schmetzer et al. 1982; Wehrmeister & Häger, 2006). The other characteristic changes of the other inclusions in corundum during a heat treatment can also be considered as indicators depending on many factors, such as the composition of inclusion, the manner of the heat treatment, the heating-up temperature, the dwelling time and the cooling rate to room temperature. The suitable heating temperature for the colour

enhancement of corundum has not a certain value. It varies in the range of 500 to 1950 °C, depending on many specifications and purposes. For example, in the case of colour enhancement, the reaction temperature of the important trace elements is required in order to gain the desired colour of corundum. But in the technique of glass filling in corundum, the right temperature is the melting temperature of glass (Milisenda et al., 2005; McClure et al., 2006). Thus, the determination of the individual applied heat treatment of corundum crystals is sometimes difficult.

As described above, the observation of inclusions in corundum crystals is considered as the best key to determine the history of any heated corundum. In a corundum host, there can be many kinds of minerals included. Which kind of mineral is included depends on the origin (Table 1.1; Hughes, 1997).

Inclusion \ Origin	Ceylon	Luc Yen	Yen Bai	Nghe An	Dak Lak	Ilakaka	Songea	Montana (Dry Cottonwood Creek)	Montana (Rock Creek)
Apatite	■								
Biotite	■	■							
Calcite		■		■					
Clinozoisite							■	■	■
CO_2	■								
Gypsum								■	
Labradorite					■			■	
Muscovite								■	
Margarite				■					
Rutile			■			■	■		■
Zircon			■		■	■			

Table 1.1 Included minerals and other phases found in corundum from various origins (Hughes, 1997).

At the present time, Madagascar is a major gem-producing country. Many gems have been exported to the gems market in the world. Corundum is a famous gem of this origin which can be found primary and secondary deposit in many parts. Primary corundum deposits of this region are hosted in magmatic (syenite and alkali basalt) and metamorphic rocks (gneiss, cordieritite, mafic and ultramafic rocks, marble and calc-silicate). Secondary corundum deposits (placers) are the most important economically and are contained in detrital basins and karsts.

Loose corundum specimen from these host rocks and soils can be used as an indicator of the geological origin by the value of the oxygen isotopic ratios ($^{18}O/^{16}O$) of itself. With this value, it is also possible to determine the primary source of the corundum from the secondary deposits. In this research, corundum crystals from Ilakaka-Sakaraha-Region which are used to study are found in the secondary deposits (Fig. 1.2). Huge variety of coloured sapphires and rubies from this area can be found in the sandstone formation in the placer but, until now, the primary host of this region is still debated because the oxygen isotope ratios of this corundum are not clear (Giuliani, et al., 2007).

The corundums from Ilakaka-Sakaraha-Region in southwest of Madagascar were first discovered around 1998. The material of this origin can often be colour enhanced by heat treatment methods. The typical colours that can be obtained with heat treatment are as stated in the following Fig. 1.3. For this study, corundum crystals with zircon inclusion from this origin were selected in order to investigate their inclusions before and after the heat treatment.

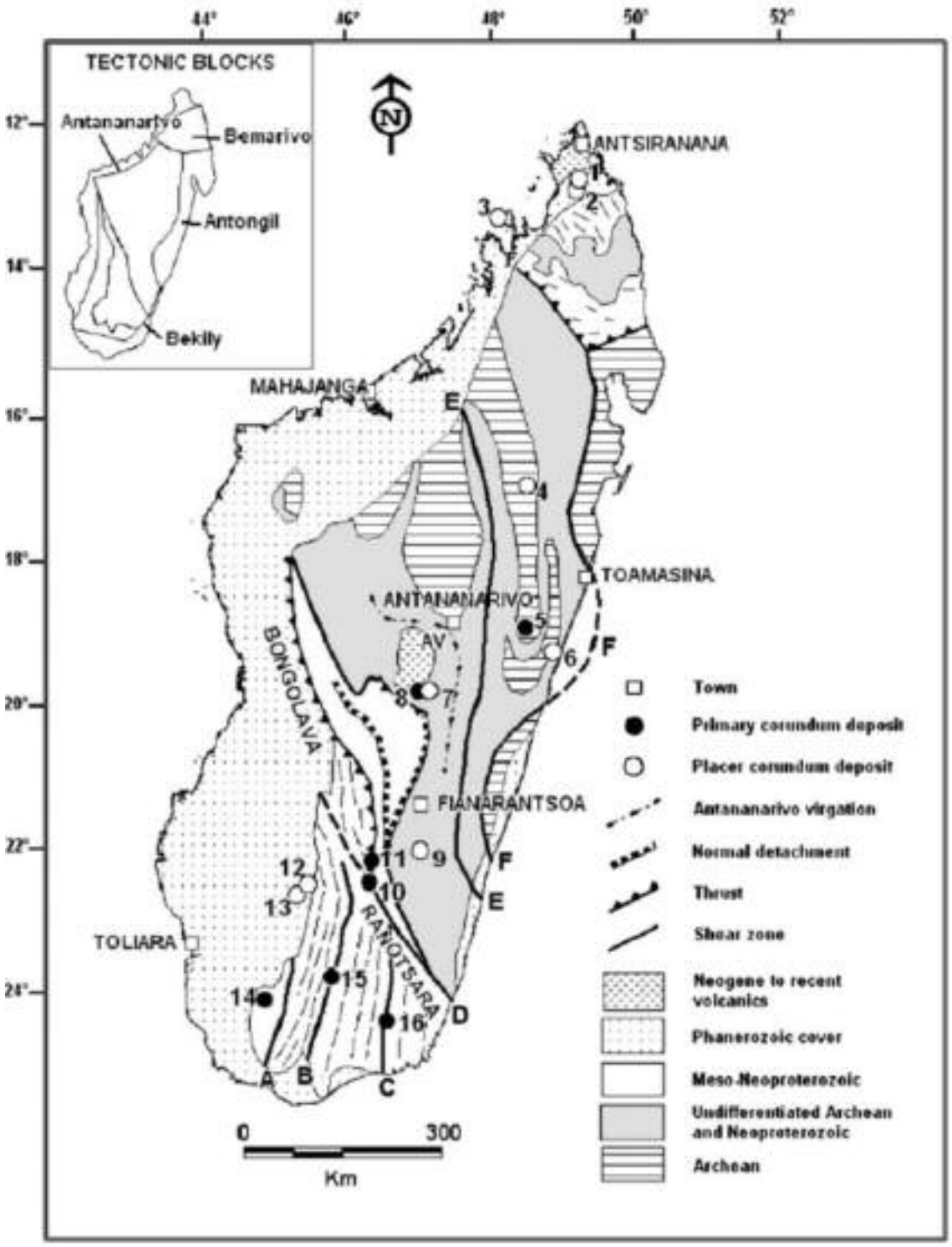

Fig. 1.2 Map showing the distribution of the primary corundum deposits and secondary corundum deposits of the gem corundum in Madagascar. Ilakaka (No. 12) which is the study area is a typical secondary deposit.

Fig. 1.3 Six corundum crystals from Ilakaka, Madagascar. The stones were cut in half for comparison. The right halves were annealed at 1750 °C (oxidizing conditions), whereas the left halves remain still in their original state for comparison (Häger, pers. Communication).

1.3 Inclusions

Inclusions are minerals and / or liquid and gas that have been trapped in the growth process of the host crystal. The trapping of inclusions has a variety of reason. A commonly reason is due to more rapid growth of the host than others mineral phases and eventually enclosing them. The inclusions in gemstones can be classified based upon their trapping character by the host into 3 types (Güberlin , 1973; Gübelin and Koivula, 1986; Hughes, 1997), as follows

1. Protogenetic, inclusions that have formed before the host.
2. Syngenetic, inclusions that have formed at the same time as the host.
3. Epigenetic, inclusions that have formed immediately after the host stopped growing, usually secondary crystallization product with liquid or gaseous inclusions.

There are many kinds of inclusions that can be found in corundum crystals, such as zircon, rutile, calcite, diaspore etc. Zircon is an inclusion that has been focused in this

study. The properties of this mineral are suitable to investigate the crystallinity and phase change after heat treatment which will be described in detail in the next part.

Diaspore (α-AlOOH) has been also focused in this research because of the similar composition to corundum after dehydration transformation process. Diaspore, which is a member of the Al_2O_3-H_2O system, becomes a stable mineral phase instead of corundum at high pressures with decreasing temperature (Fig. 1.4; Deer et al., 1962; Levin et al., 1964; Giuliani, 2003). Therefore, diaspore can be found as a secondary or daughter mineral as inclusion in corundum crystals.

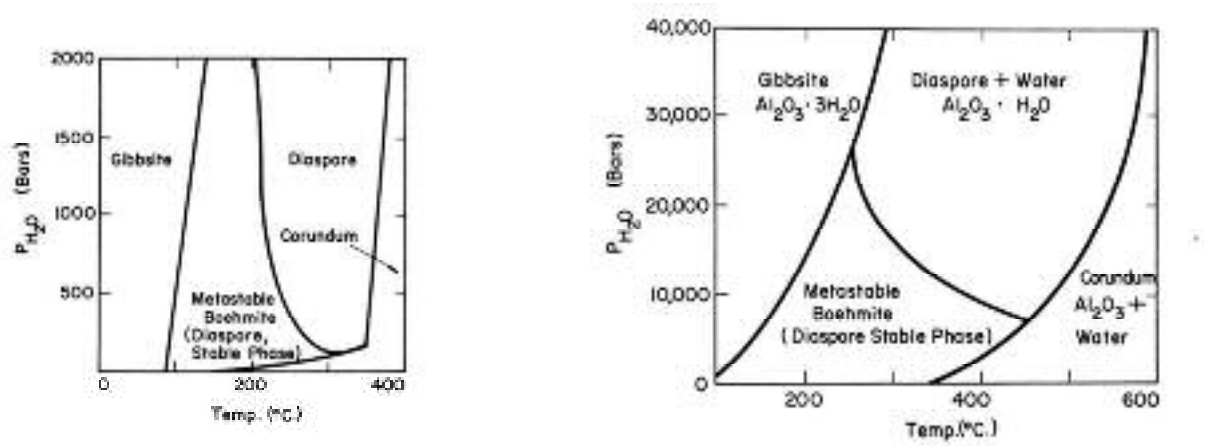

Fig. 1.4 Phase diagram of Al_2O_3 with H_2O showing the variation of the aluminium hydroxide minerals at different pressures and temperatures (Levin et al., 1964).

Diaspore particles have been found as inclusion in Sri Lankan corundum (Schmetzer and Medenbach, 1988) and this kind of inclusion can be transformed to corundum by heat treatment (Ervin, 1952; Carim et al., 1997). With this property, the diaspore inclusion should not be found in a heated corundum crystal, but the temperature of the actual phase transformation of this inclusion has not been reported. This temperature will be investigated in this study.

1.4 Zircon

Zircon can be found as a common accessory mineral in many types of rocks (Klein and Hurlbut, 1993). It occurs as a primary crystallisation phase in many igneous rocks, as xenocrysts in mafic and ultramafic volcamic rocks, and as recrystllized grains in various types of metamorphic rocks (Guo, et al., 1996). This mineral, moreover, contains the rare earth elements (REE) which have been recorded as fingerprints from their parent magma (Heaman, et al., 1990). Consequently, this geochemical signature of the zircons can identify their parent source rocks (Guo, et al., 1996; Sutherland, et al., 1998). In addition, there is not only the REE contained in zircon but also radioactive elements may be contained in its structure which is also an important property of this mineral.

Zircon can be found as an inclusion in corundum crystal. In the forming of minerals within the Al_2O_3–SiO_2–ZrO_2 system, when Al_2O_3 is less reactive, $ZrO_2.SiO_2$ crystallizes to zircon ($ZrSiO_4$) under a suitable pressure and temperature. When this environment is changed to the enriched Al_2O_3 composition, corundum crystallizes. If the corundum grows rapidly, the remained zircon crystal in this environment can be trapped as an inclusion in the corundum.

As shown in Table 1.1, zircon is always found as mineral inclusion in corundum crystals from the Ilakaka-Sakaraha-Region (Milisenda et al. 2001; Sakkaravej et al., 2005; Wang et al. 2006). This mineral, nowadays, is extensively investigated by many mineralogists. It is widely used in many industries and it has a major role as potential host materials for radiogenic waste materials (Ewing, 1999; Wang et al., 1999; Colombo et al., 1999; Rios and Boffa-Ballaran, 2003). The structure of zircon ($ZrSiO_4$, $I^{41}/_{a}md$ and Z = 4; Hazen and Finger, 1979) shows it to be a nesosilicate (or orthosilicate) crystallizing in the tetragonal system with a c/a ratio of around 0.906 (Knittle and Williams, 1993). The zircon composition and crystal structure were redetermined, recently by Harley and Kelly (2007). The ideal structure of zircon consists of the ZrO_8 polyhedra, extending parallel to the c-

axis, linked with the two opposite edges to SiO_4 tetrahedra and the four others at the corner of two perpendicular planes (Fig. 1.5). Hafnium (Hf, ionic radius = 0.83Å) is always found in small amounts in the zirconium position. Zircon crystal also contain radioactive elements in there structure, such as uranium and thorium. The Zr^{4+} (0.084 Å) cation can be substituted by U^{4+} (0.10 Å), Th^{4+} (0.105 Å) and with lead (Pb, 0.129 Å) as the end member of the series. Moreover, Ti^{4+} (0.074 Å) can be also accommodated, but in the low abundance level.

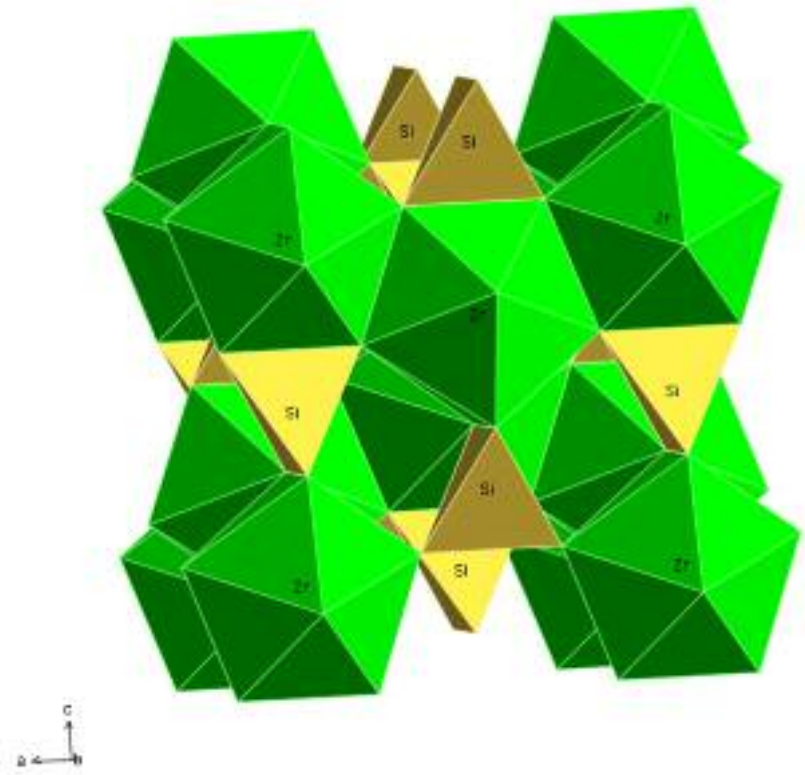

Fig. 1.5 A view of the structure of zircon ($ZrSiO_4$) parallel to the b-axix, showing the ZrO_8 polyhedra and SiO_4 tetrahedra.

^{238}U has eight alpha-decay steps before becoming the stable isotope ^{206}Pb, seven steps for ^{235}U to ^{207}Pb and six steps for ^{232}Th to ^{208}Pb. The decay of these radioactive elements produces the common types of radiation as alpha, beta, and gamma. Beta and gamma radiation can be negligible for the production of structural damage. But most of

alpha particles lose their energy through ionisation in the host structure. This action slightly causes damage of the host structure but may process high long-term stability which can be seen in the damage haloes in biotite (Gentry, 1974; Nasdala et al., 2001b; Nasdala et al., 2005). However, the recoiled daughter nuclei produced upon emission of an alpha particle can generate even a higher localized structural damage cluster (Nasdala et al., 2005), which is known as metamictization. This phenomenon impacts the density values of zircon, which ranges from 4.70 to 3.90 g/cm^3, accompanied by a clear change of optical properties like refractive indices. The range of physical constants fluctuation is influenced by the degree of the deformation and damage of the zircon structure affecting to the unit-cell expansion (Özkan, 1976; Trachenko et al., 2002; Rios et al., 2003).

For metamict zircons, a degree of heterogeneously activated damage can be found commonly in natural zircon crystals. This distribution relates to the inhomogeneous content of the radioactive elements. The high radioactive content area usually shows relatively high degrees of metamictization (Nasdala et al., 1996). In addition, the metamictization area may decompose to zirconia (ZrO_2) and a silica (SiO_2) phase depending on the influence of locally acting radiation (Özkan, 1976; Colombo et al., 1999; Zhang et al., 2000a, b). To measure the degree of metamictization, many methods have been investigated and applied. Among them, Raman spectroscopy is applied very successfully as it is a non-destructive method which acts straight forward to determine the degree of metamictization (Nasdala et al., 1995).

1.5 Diaspore and other aluminium hydroxide minerals

Diaspore is an orthorhombic (Pbnm) hydroxide mineral in the goethite group which commonly is associated with corundum in natural occurrences. The crystal structure of diaspore shows chainlike patterns of octahedrally coordinated cation sites occupied by Al^{3+} extending along the c-axis (Fig. 1.6). Each chain shares edges of the octahedral sites with other chains and the chains are joined to each other by adjoining apical oxygen anions. The oxygen anions and the $(OH)^-$ groups are arranged in hexagonal closest packing, resulting in the octahedral coordination of the cations (Klein and Hurlbut, 1993).

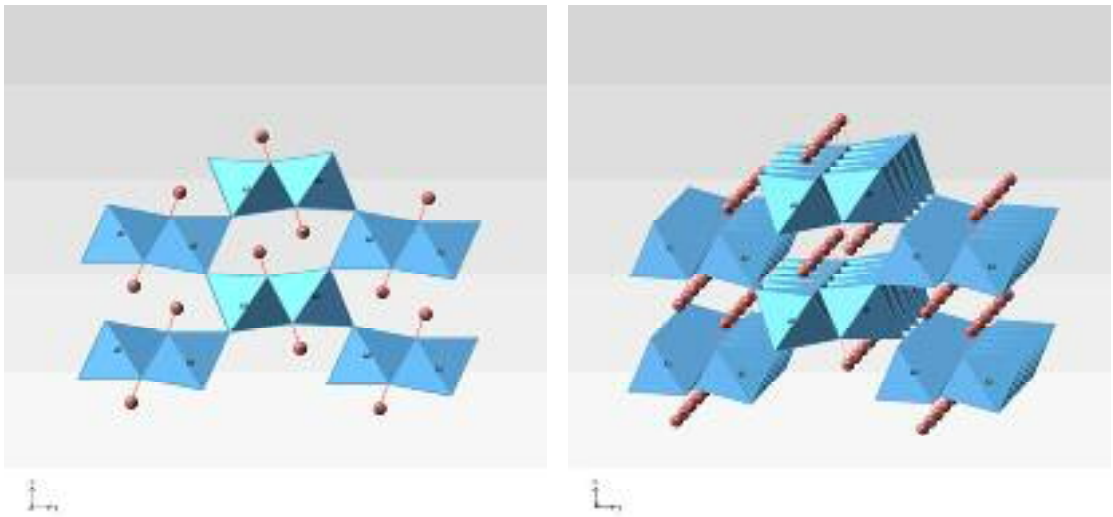

Fig. 1.6 Diaspore crystal structure showing chainlike patterns of octahedrally by OH-anions coordinated Al^{3+} - cations extending along the c-axis.

Not only diaspore, but also a number of other aluminium hydroxide minerals is associated with Al_2O_3 minerals such as boehmite (γ-AlOOH), gibbsite (γ-$Al(OH)_3$), and bayerite (α-$Al(OH)_3$) depending on pressure and temperature of formation (Fig. 1.4). Boehmite is a polymorphic mineral to diaspore. The difference of these two minerals is the packing of the oxygens which is the cubic closest packing for boehmite (Fig. 1.7; Ervin, 1952). The crystal structures of gibbsite and bayerite bear the same sheet-like units, which consist of a layer of aluminium ions sandwiched between two layers of hexagonally

packed hydroxyl ions in the plane defined by the a and b axes, but they have different sequence of the layers by a rotation parallel to the c axis of one of the sheet-like units by 60° (Giese, 1976; Ruan et al., 2001). All of these hydroxide minerals can be transformed to anhydrous alumina compounds with the α-Al_2O_3 structure by heat treatment (Ervin, 1952, Broesma et al., 1978, Carim et al., 1997, Temuujin et al., 2000).

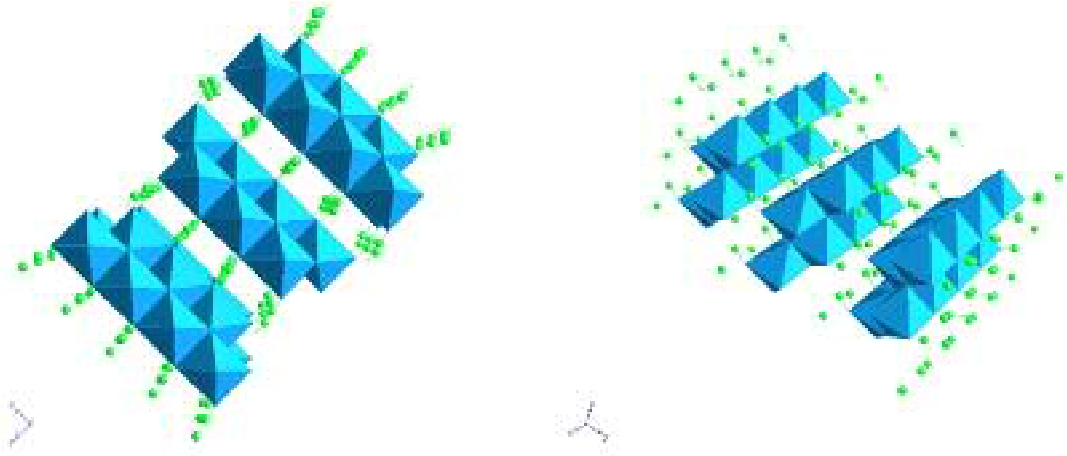

Fig. 1.7 Boehmite crystal structure with the cubic clostest packing of the oxygens which is a polymorphic mineral to diaspore.

2. Reactions and analyses during heat treatment

2.1 TG and DTA

Nowadays, heat treatment is a wide spread method to enhance the colour of corundum crystals. Suitable temperatures used for the colour treatment of corundum species varies in the range of 500°C to 1950°C, depending on many specifications and purposes. As mentioned above, the aluminium hydroxide minerals can be found as daughter minerals in corundum which can be transformed to corundum during the heat treatment. Therefore, these minerals should not be found in heat treated corundum crystals. However, the transformation temperature of these minerals as an inclusion in corundum has not been exactly reported. In this experiment, thermogravimetry (TG) and Differential Thermal Analysis (DTA) were used to determine the transformation temperature of these hydroxide mineral inclusions within the corundum host crystals.

Thermogravimetry, TG, is an analytical method to study the weight losses of samples during heating experiments. With this method, the result will register the beginning and the ending temperature of the weight losses of the sample and the amount of weight lost at a certain temperature. Differential Thermo-Analysis, DTA, is a measurement method for evaluating the energy change in the material investigated during heat treatment. The basic concept of this method is to compare the energy change between an inert and well known reference material (in our case corundum) and the samples which are annealed with the same increasing temperature rate in the same furnace. The reference material which has no physical and chemical change is chosen to compare with the sample under the same conditions. When there is a phase transition in the sample, such as melting, the measured temperature of the sample will lag behind because of the absorption of the energy of the sample (endothermal). This result will be shown in the DTA curve. On the other hand, if there is a heat-producing (exothermal) reaction by the sample, the opposite result of the curve will be shown.

2.2 Raman Spectroscopy and Fluorescence Spectroscopy

Raman spectroscopy is a vibrational spectroscopy based upon the Raman Effect described as the scattering of light from a gas, liquid or solid with a shift in wavelength from the monochromatic incident radiation. When a sample was irradiated with a monochromatic light, not only the exciting frequency is observed (Rayleigh scattering (ν_0), elastic light scattering with no change in energy) but also some weaker bands (certain loss of energy of a material due to molecule vibration) shifted in energy from the Rayleigh line are detected. These weaker bands can be found on both sides of the Rayleigh and the scattering lines are called Stokes and anti-Stokes (Fig. 2.1). Stokes is the lower frequency shift (ν_0-ν_i) and anti-Stokes is the higher frequency shift (ν_0+ν_i) from the incident wavelength. The intensity of Stokes bands is much stronger than the anti-Stokes bands, which is usually used to determine the molecule vibration bond of the materials used the experiment.

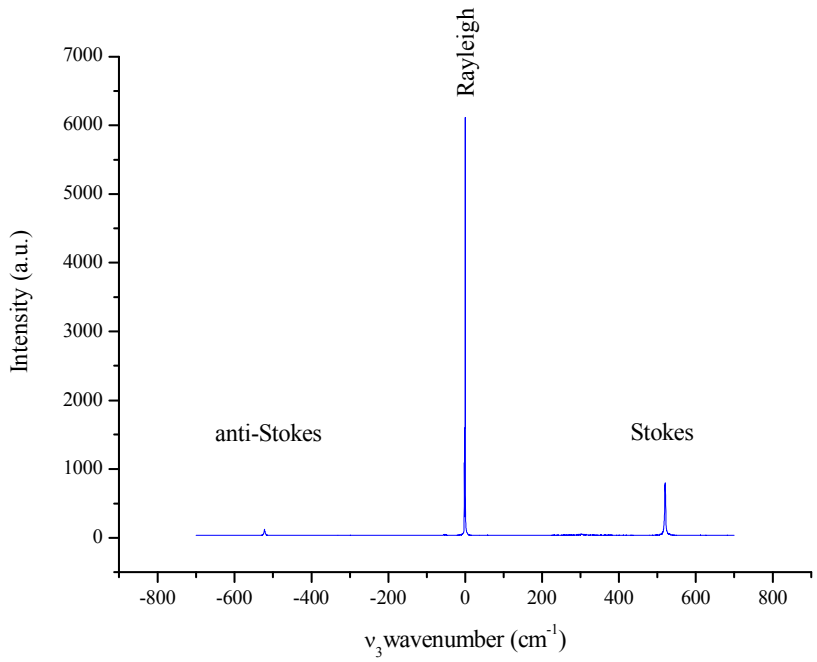

Fig. 2.1 Rayleigh and Raman bands of Stokes and anti-Stokes line of silicon wafer excited with the Helium-neon laser (632 nm).

This Raman shift provides information about vibrational, rotational and other molecular modes. With this information, Raman spectroscopy can be used to study mineral phases and crystallinity of material (McMillan and Hofmeister, 1988). Under the pressure, moreover, the molecules vibrations are distorted inducing the higher Raman shift than at ambient pressure (Lam, et al., 1990).

A fluorescence emission phenomenon responds in the material under investigateion to the incident radiation similar to Raman scattering. This emission may be from the bulk of the material itself, or from isolated impurities, clustered defects, exsolved phases, included phases, or grain boundary contaminants. This process involves the transition of an electron from excited state (conduction band) to one lower energy state, which was excited from the ground state (valence band) to the excited state (Fig. 2.2). The return of electron involves non-radiative transitions (absorption or emission of lattice vibrations) and radiative transitions (the emission of light photons) on a particular crystallographic site, largely independent of the rest of the host structure. Therefore, the energy difference between the absorbed and emitted photons ends up as molecular vibrations or heat, causing the emission of fluorescence at a longer wavelength (Waychunas, 1988; Nasdala, et al., 2004; Gaft, et al., 2005).

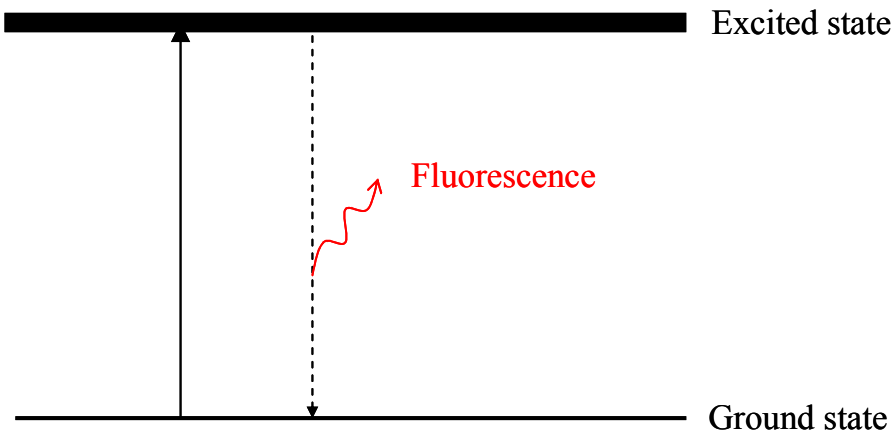

Fig. 2.2 Simplified sketch of the electronic band structure showing the transition of an electron from excited state to one lower energy state causing the emission of fluorescence at a longer wavelength.

In comparison between the Raman scattering and fluorescence emission, the fluorescence band can be found only in the Stokes line and this band is controlled by the energy difference between excited state and ground state of the fluorescence material. Therefore, the fluorescence band can be found at the exact wavelength position. In contrast with the Raman band, which has a certain loss of energy of a molecule vibration, it shifts with the exact wavenumber from the incident radiation wavelength.

It is well known that fluorescence of the corundum is caused by the substitution of Cr^{3+} in the Al^{3+} octahedral sites. To produce the fluorescence in Cr^{3+} containing corundum, there are three energy levels at hand. The incident laser beam excites the electron to the absorption levels which is a spin allowed transition ($^4T_{1g}$ and $^4T_{2g}$; Fig. 2.3; Tanabe and Sugano, 1954). The lifetime of these levels is short (50ns), then excited ions quickly relax by perfoming a transition to a long-lived metastable state (^2E_g). The energy which is lost in this process is non-radiative and produces purely heat. This cubic field of this state is split to the both lines due to the trigonal distortion of the octahedral site and the spin-orbit coupling (see the inset in Fig. 2.3; Nelson and Sturge (1965); Eggert, et al. (1989); Häger and Dzung (2003)). The transition from the ^2E_g state to the ground state involved, is the spin forbidden $^2E \rightarrow {}^4A_2$ transition within the d^3 configuration of the Cr^{3+} ions subject to the crystal field of the surrounding oxygen ligands (Patra, et al., 2005). The doublet emission sharp lines at 694.2 and 692.8 nm (R_1 and R_2 at room temperature) are produced which due to the different energy between these states. The lifetime of these R-lines is 3.5 ms (Heiman, 2007).

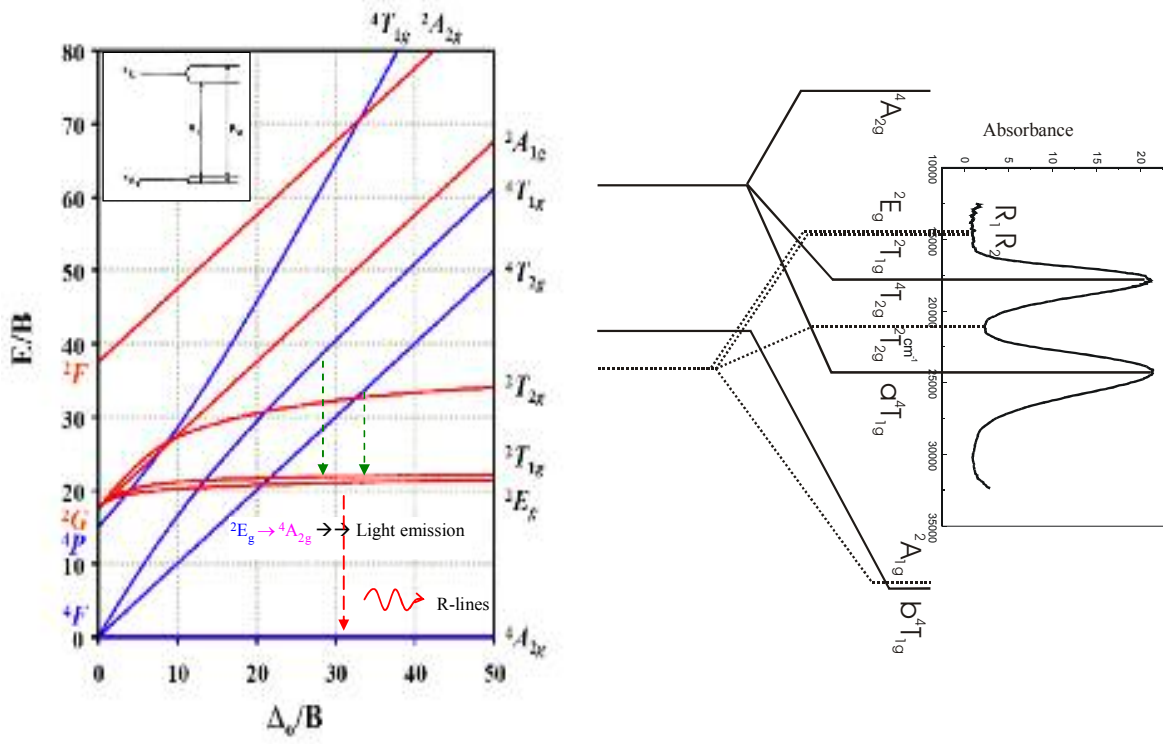

Fig. 2.3 Left, Tanabe-Sugano diagram showing the spin forbidden $^2E \rightarrow {}^4A_2$ transition within the d^3 configuration of the Cr^{3+} in the corundum structure. Inset shows the doublet fluorescence sharp lines at 694.2 and 692.8 nm (R_1 and R_2 at room temperature) due to the trigonal distortion of the octahedral site and the spin-orbit coupling (modified from http://chemistry.bd.psu.edu/jircitano/TSdiagram.pdf (2007), after Tanabe and Sugano, 1954) . Right, UV-vis spectra shows the absorption bands of ruby and the emission band of R-lines (Tobias Häger, personal communication, 2007).

In case of corundum under pressure, the strain affects to the distortion of the trigonal field inducing the shift of the R-lines (Sharma and Gupta, 1991; Shen and Gupta, 1993). With this property, the fluorescence of the Cr^{3+} doped corundum is used to calibrate the experimentally pressure in a diamond anvil cell experiment (DAC).

2.3 Determination of the metamictization degree by Raman spectroscopy

The estimation of the metamictiztion degree of zircon by Raman spectroscopy was first reported by Nasdala, et al. (1995). They concluded that the high degree of metamictization is caused by the increase of irregularities of bond-lengths, bond-angles and a general breaking-up of the structure by the self-irradiation of the radioactive elements. Those effects can be determined by the changing of the Raman-Peak positions and the full-width at half maximum (FWHM) of the antisymmetric stretching vibration band (B_{1g}) of the SiO_4 tetrahedra. This B_{1g} band is the most sensitive Raman band of zircon at around 1000 cm^{-1}, which is, nowadays, usually applied to determine the metamictization degree of zircon, and it is called "ν_3 band" (see Fig. 2.4).

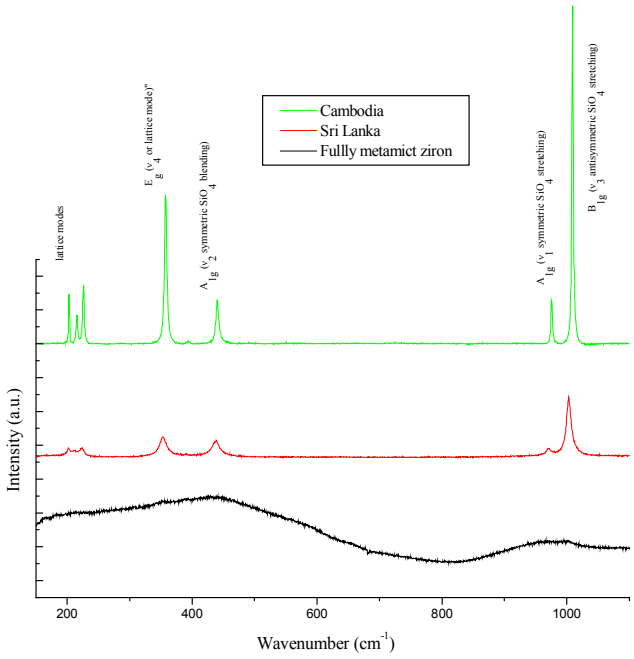

Fig. 2.4 Raman spectra of various zircon samples. The zircon from Cambodia (upper spectrum) shows minor radiation damage and the zircon from Sri Lanka (middle) moderate one. The green stone (unknown origin) is close to be completely of amorphous state, indicating the highest degree of metamictization.

For the estimation of the degree of structure damage in zircon, the FWHM of the ν_3 band is focused. The FWHM of crystalline zircon is around 2 cm^{-1}, whereas the FWHM of the moderately, as well as highly, damaged degree is boarder than 25 cm^{-1} (Nasdala et al., 2002 a, b). The Raman bands of metamict zircon show not only the obviously broader FWHM, compared with the well crystalline zircon, but also the decrease of the Raman bands position, e.g. for ν_3 from 1007 cm^{-1} to 955 cm^{-1} of the well-crystalline zircon to the highly metamict one, respectively (Nasdala et a., 1995). The strongly damaged structure of a highly metamict zircon, resulting from the damage of the well-ordered lattice structure by the irradiation, is presented in the form of the broad Raman bands (the lowest spectrum in Fig. 2.4).

The locally damaged crystal structure of metamict zircon can be recovered by heat treatment (Özkan, 1976; Mursic, et al., 1992; Colombo et al., 1999, Capitani et al., 2000; Zhang et al., 2000a, b and Nasdala et al., 2001, Nasdala, et al., 2002a; Geisler, 2002; Rios and Boffa-Ballaran, 2003; Westrenen, et al., 2005). This recovery is a common phenomenon in natural zircon crystals under the influence of high temperature. This phenomenon has been investigated to understand the phase change and recrystallization mechanism. There are some publications reporting about annealed zircon and the recovery of the damaged structure, determinable with Raman spectroscopy (Zhang, et al, 2000a, b; Nasdala, et al., 2001; Nasdala, et al., 2002a, b; Geisler and Pidgeon, 2002). They concluded that, through annealing, the highly metamict zircon can transform into the crystalline zircon. This recrystallization can be observed by the ν_3 Raman band, which shows the decrease of the FWHM from the broader band of metamict zircon to the narrower band of crystalline zircon. Moreover, the Raman position of this band also increases after recrystallization because of the recovery of the damaged lattice structure. The annealing temperature was varied by Nasdala et al. (2002a), concluding that, in highly metamict zircon, the recovery does not start significantly below 800 °C. The amorphous

structure of $ZrSiO_4$ was changed to a ZrO_2 phase after annealing at 950 °C. At 1100 °C, $ZrSiO_4$ is the main phase and ZrO_2 becomes minor. The ν_3 band of zircon shifts to the higher wavenumber of 1011 cm^{-1}, which is 2 cm^{-1} higher than the Raman shift position of the well crystalline zircon. Nasdala, et al. (2002a) explain this by the compressive strain in the small $ZrSiO_4$ particles, which increases by the decreasing of particle size. The result of the zircons annealed at 1250 °C shows only minor variations compared with synthetic zircon. From these results, it can be concluded that a heat treatment at this temperature range does not cause major changes of the mineralogical composition of the zircon and its inclusions.

Furthermore, many research projects are involving only the annealing of free standing metamict zircon under ambient pressure, except the reports of Wang et al. (2006), and Wanthanachaisaeng et al. (2006d). Wang et al. (2006) studied the effects of the heat treatment on zircon inclusions in Ilakaka corundums in the temperature range from 1400°C to 1850°C. They concluded that most of the inclusions in the corundum host are metamict zircon inclusions before heat treatment and they found relatively high pressure values (up to 27 kbar) around the inclusions due to metamictization. The progressive decomposition of zircon inclusion in the corundum host occurred at temperatures between 1400°C and 1850°C. The beginning of the decomposition of zircon into baddeleyite (ZrO_2) and a SiO_2-rich phase occurred at the temperature as low as 1400°C. The melting of zircon can be observed in the inclusions at 1600 °C and above. The Raman shift of the ν_3 band was also reported in this study. This band of the unheated zircon was in the range of 1014-1021 cm^{-1}. It shifted, after being heated, to the higher wavenumber. For the FWHM, the unheated zircon inclusions have the FWHM of the crital band in the range of 10.1-13.5 cm^{-1}. After heat treatment, the average value is around 8 cm^{-1}, indicating the recovery of the damaged structure. At high temperature, the molten inclusions show tiny dendritic-like quenched crystals of m-ZrO_2 (baddeleyite) and a SiO_2-rich phase, which was the similar result as of

Rankin and Edwards (2003). Hf, which can be found as a minor element in the zircon inclusion does not affect the shift of the zircon Raman band.

2.4 Determination of the internal pressure by quantifying the Cr^{3+} fluorescence

Nowadays, the investigation of the internal pressure associated with coexisting minerals has been extensively studied by many methods. The well known method to determine the pressure of minerals being under high pressure in a diamond anvil cell (DAC) uses of the Cr^{3+} fluorescence in ruby according to a pressure calibration (King, 1978; Wunder et al., 1981; Jayaraman, 1983; Malinowski, 1987; Piermarini, 2001). The DAC is also applied in order to calibrate the shift of Raman bands under high pressure. The pressure-induced phonon frequency shift of the minerals under investigation, measured by Raman scattering, has been used as a pressure sensor (Mitra, et al., 1969; Tardieu, 1990; Knittle and Williams, 1993, Wang et al., 1993; Izraeli et al., 1999; Schmidt and Ziemann, 2000; Sobolev et al., 2000; Chen et al., 2004; Nasdala et al., 2005). Both of these pressure sensors can be used to estimate the pressure of the mineral under high pressure as a non-destructive method.

The shift of the ν_3 Raman band, which is focused on this study, was also reported by Knittle and Williams, 1993. They concluded that the phase transition of the $ZrSiO_4$ from the zircon structure to the scheelite structure occurs at 230 ± 10 kbar at 26.85 °C. The ν_3 band at 1006 cm^{-1} shifts to the higher wavenumber under high pressure in the ratio of 4.8 ± 0.2 cm^{-1} per kbar. With this constant, the trapped pressure between zircon inclusion and corundum host was calculated by Wang et al. (2006).

The trapped pressure between the zircon inclusion and the corundum host can be measured by the shift of ν_3 band of the inclusion as described above. In this study, however, the determination of the pressure between the inclusion and host crystal was investigated with the shift of the Cr^{3+}luminescence. Corundum often contains Cr^{3+}, which

is the cause of the red colour (ruby) and simultaneously the cause of the luminescence phenomena. The luminescence emission spectra of Cr^{3+} in corundum are dominated by two major emission, R_1 and R_2 bands as described in Fig. 2.3 (page 17).

There are many publications dealing with the pressure dependence of the ruby R_1 band because it is used as a barometer in high pressure experiments (Powell et al., 1967; Piermarini et al., 1975; Munro et al., 1985; Mao et al., 1986; Liu et al., 1988; Horn and Gupta, 1989; Eggert et al., 1989a, b; Eggert et al., 1991; Gupta and Shen, 1991; Yen and Nicol, 1992; Shen and Gupta, 1993; He and Clark, 1997; Jovanic, 1997; Yu and Clarke, 2002; Nasdala et al., 2004) . Piermarini et al. (1975) concluded that at 25 °C under compression in NaCl, the pressure can be determined by the shift of the wavelength following the equation

$$P_{NaCl}=2.746(\Delta\lambda),$$

where P is the pressure in kbar and $\Delta\lambda$ the shift in Å. Mao et al. (1986) also proposed the following equation to calculate the pressure with

$$P = (A/B)*[(1+ \Delta\lambda / \lambda_0)^{B}-1]$$

where A= 19.04 Mbar, B= 7.665 and $\lambda_0 \approx 6942.8$ Å and $\Delta\lambda$ is again the shift of the R_1-band also in Å. With these literatures data, it can be concluded that the shift of R_1 band is approximately 1 Å for 2.74 kbar (Fi. 2.5).

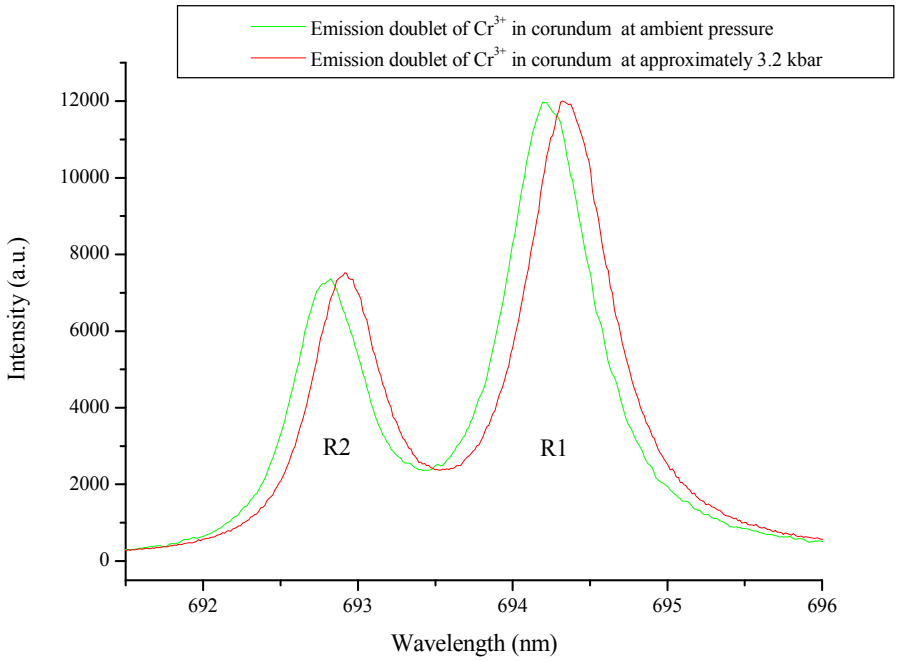

Fig. 2.5 Fluorescence emission doublet of Cr^{3+} in corundum at ambient pressure (green spectrum) and approximately 3.2 kbar (red spectrum).

The pressure difference between inclusion and host depends on the bulk modulus and the thermal expansion coefficients. Izraeli et al. (1999) described two cases of inclusions:

1. No pressure, when the final volume of the inclusion is smaller and
2. Under pressure, when the final volume of the inclusion is larger than the hole in which it is situated.

The pressure around different types of inclusions may vary in a single host (Zhang, 1998). The crystallographic orientation of the host and the inclusion has also an influence on the pressure between them (Ragan et al., 1992).

The residual pressure of the graphite inclusion in diamond was reported recently by Glinnemann et al. (2003) and Nasdala et al. (2003). They found that the residual pressure of graphite inclusion from Ekati, Canada, is approximately 24 kbar by calculations

following single crystal diffraction experiments and approximately 26 kbar by the shift position of Raman band, respectively.

With these 2 methods, the pressure between the minerals can be determined by both Raman shift and luminescence shift (Wanthanachaisaeng et al., 2005). In this study, the shift of R_1 luminescence has been applied to measure the trapped pressure between inclusion and the Cr^{3+} containing corundum host, comparing it with the shift of ν_3 band of the unheated and heated corundum.

3. Methods and Materials

3.1 TG and DTA experiments

In the first experiment, powder of diaspore, boehmite, gibbsite and bayerite and a massive translucent ruby single crystal sample from unknown origin (Fig. 3.1), which could contain unknown hydroxide minerals, were heated from room temperature to 1200°C with a heating rate of 10 °C/min with the NETZSCH STA 429 CD (Simultaneous thermogravimetry–differential scanning calorimetry, Fig. 3.2). Powder of α-Al_2O_3 was used to be the reference material. The results of TG and DTA measuring procedures show the phase change of aluminium hydroxide minerals to aluminium oxide. Then, these results will be compared with the ruby result to determine the type of included minerals.

Fig. 3.1 Ruby sample from unknown origin used in this experiment.

Fig. 3.2 Simultaneous thermogravimetry–differential scanning calorimetry (NETZSCH STA 429 CD).

3.2 Raman spectroscopy and Fluorescence spectroscopy

Raman spectroscopy and fluorescence spectroscopy were used in this experiment. The results of Raman and fluorescence spectroscopy were obtained by a Jobin Yvon LabRam-HR 800 Raman microprobe, which is equipped with an Olympus optical BX41 microscope (with 50x long working distance objective; numerical aperture 0.55) (Fig. 3.3). The spectra were excited with the Argon ion 514.5 nm wavelength Laser-light. The advantage of this wavelength is that the Raman peaks and the luminescence peaks are far away from each other and can be determined separately. Also, this laser was used in fluorescence spectroscopy (35 mW). These spectra were collected by a CCD detector and were obtained by confocal measuring technique with a grating of 1800 grooves per mm, slit width of 100 μm. The wavenumber accuracy is ± 0.5 cm^{-1} with the spectral resolution approximately at 0.8 cm^{-1}. The laser beam has been focused to the sample volume in the confocal mode. This mode contains an aperture at a back focal plane of the microscope to

improve the lateral and axial spatial resolution and remove the information from the out of focus area. With this confocal mode, the data can be measured deeper under the surface (in the range of 10 μm) (Baldwin and Batchelder, 2001; Everall, 2004a, b. The accuracy of the luminescence measurement was calibrated by the series of Rayleigh-line and the emission of a Neon-light. The counting time used in these experiments varied between 1 to 60 second and all measurement was twice in order to eliminate spikes. The results of the band positions, the maximum intensity and the FWHM data of the Raman and luminescence bands were calculated by the combination of Gaussian and Lorentzian functions after background correction (Munro et al., 1985, Nasdala et al., 2005).

Fig. 3.3 The Jobin Yvon LabRam-HR 800 Raman microprobe equipped with Olympus optical BX41 microscope and controlled by a motorized, software-controlled x-y stage.

In order to determine the trapped pressure, the shift of Cr^{3+} luminescence bands method (Wanthanachaisaeng et al., 2005) was applied in this study. The R_1 luminescence band shifts with 0.1 nm per 0.274 kbar. This band shift is linear with increasing pressure up to 195 kbar (Barnett et al., 1973; Piermarini, et al., 1975). The R_1 band may also be shifted by the variation of temperature in the magnitude of about, 7.4 x 10-3 nm/K (Yen and Nicol, 1992). Then, it might be possible to get pressure data below 0 kbar after calculating data. However, the pressure that is measured in this study is the relative pressure between the matrix of host corundum and the boundary of the inclusion. Therefore, the maximum pressure is the different pressure of the both objects.

The calculation was done automatically by the Labspec software (Horiba Jobin Yvon) with the curve fitting procedure by the combination of Gaussian and Lorentzian functions. The concentration of the Cr^{3+} in the corundum host, and the orientation of the corundum were ignored in this experiment because the relative shift between the matrix and the inclusion area only were analysed. To analyse the pressure distribution, the mapping technique was used. The mapping technique means, each spectrum is obtained in succession of x- and y-coordinate changes software-controlled by the sample stage. The fluorescence spectra were accumulated from the selected areas. More than 30000 fluorescence spectra were analyzed per measuring sequence and the shifts of R_1 were transferred into a colour-coded image. Every pixel in the colour-code map represents one fluorescence spectrum. The areas analyzed, measured approximately 200 x 300 μm.

3.3 The scanning electron microscope

A Zeiss 962 Scanning Electron Microscope (SEM), equipped with the Oxford Instrument Energy Dispersive X-ray (EDX) spectrometer, was used to analyse the zircon inclusion exposed at the surface of the corundum host crystals after being heated at 1800°C. A thin layer of carbon was coated over a polished surface of the host sapphire to improve

electrical conductivity. The back scattering image of the decomposed inclusion was recorded at the magnification up to 800x using an accelerating voltage of 15 kV.

3.4 Zircon inclusions and host sapphire samples

Corundum crystalsfrom Ilakaka, Madagascar, with the zircon inclusions, which are dominant in this origin, were selected for this study. One of these corundums, containing 40 ppm of Cr^{3+}, was heat-treated with an electric furnace oven in oxidizing condition (air) (Fig. 3.4). With the heating rate of 10°C per minute, each sample was heated at 500, 800, 1000, 1200, 1400, 1600, and 1800°C for 3 hours at each target temperature. After each heating experiment, the sample was immediately taken out of the oven in order to investigate the zircon inclusions by Raman and Luminescence spectroscopy.

25 samples of the zircon inclusions in unheated corundums were determined, aiming at the degree of metamictization and the trapped pressure between the inclusions and host corundum by Raman spectroscopy and fluorescence spectroscopy, respectively. Three zircon inclusions (mi7c, mi7d and mi7e) in a green sapphire sample (mi7; Fig. 3.4) have been investigated in order to see the phase change of the inclusions during heat treatment (Fig. 3.5). These inclusions are transparent and were in the average size of approximately 50 μm. Their degree of metamictization and the trapped pressure were also determined. These experiments are also done on the same inclusions after being heated at each target temperature.

In this study, moreover, two zircon single crystals from Cambodia and Sri Lanka, and a faceted zircon from an unknown origin have been used as reference materials with different degrees of metamictizaiton for better understanding the spectral features of the inclusions behaviour (Fig. 3.6).

Fig. 3.4 Green sapphire with zircon inclusions from Ilakaka, Madagascar.

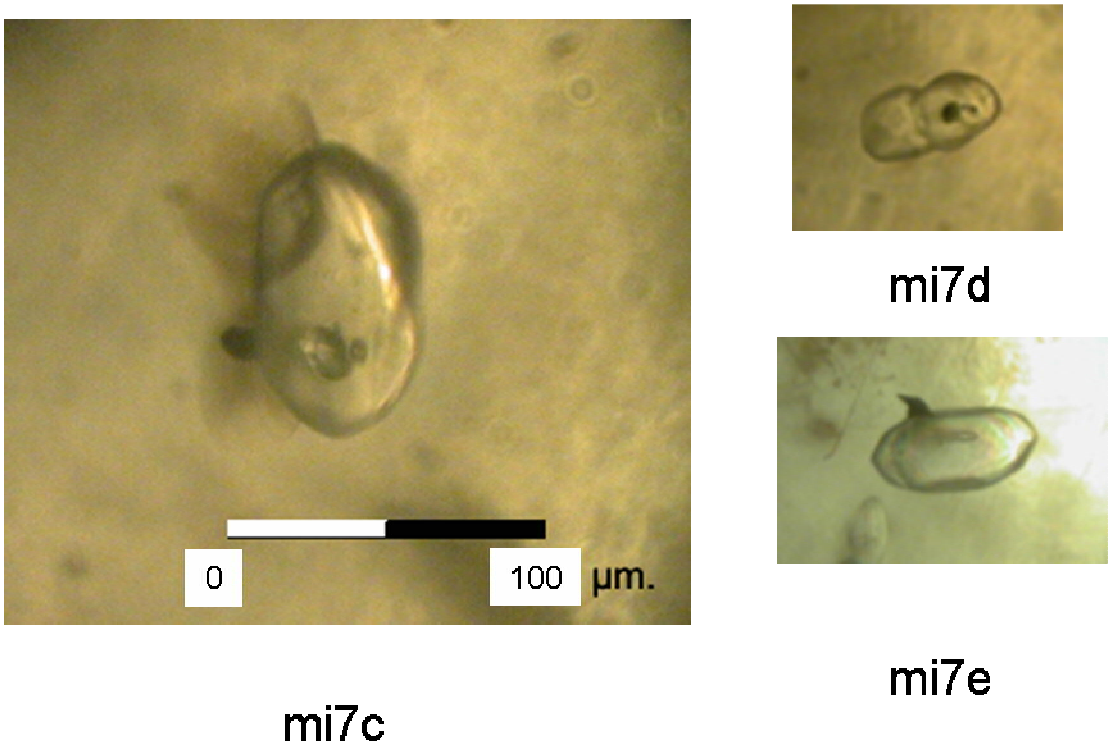

Fig. 3.5 Three unheated zircon inclusions in a green sapphire from Ilakaka, Madagascar (Fig. 3.4) were selected and heated to investigate the phase.

Fig. 3.6 Zircons from Cambodia and Sri Lanka, and an irradiated zircon from unknown origin (from right to left, respectively) used as the references for the degree of metamictization.

4. TG and DTA results

The results of the heating experiments on the aluminium hydroxide minerals and the ruby sample are represented by the patterns of weight loss in the TG curves and endothermic bands in DTA curves. The TG results are shown in Fig. 4.1. Interpreting the results, they can be divided into 2 mineral groups based on the difference of initial weight loss with increasing temperature. The first group contains the mineral phases diaspore and boehmite and the second group contains bayerite and gibbsite. The weight loss of diaspore began at around 420°C and the weight curve shows as normal decreasing slope and ends the decreasing of weight at around 570°C. Boehmite shows a similar diagram to diaspore. The weight loss temperature starts at around 380°C, but with a steeper slope and a decrease until the end at around 580°C. This steeper slope illustrates the more rapid change of the weight loss caused by the different crystal structures.

On the other hand, bayerite and gibbsite show different results in comparison to the TG curves of the first group. Bayerite began to loose weight at a lower temperature, compared with the initial weight loss of diaspore and boehmite, at around 230°C and ends at around 320°C. Gibbsite begins with weight loss at around 225°C with a steeper slope than bayerite and ends at around 305°C. All of these minerals loose weight at the same ratio of around 12 % after annealing because of the loss of water and volatile impurities within their structure. All of the heated samples have been changed to α-Al_2O_3.

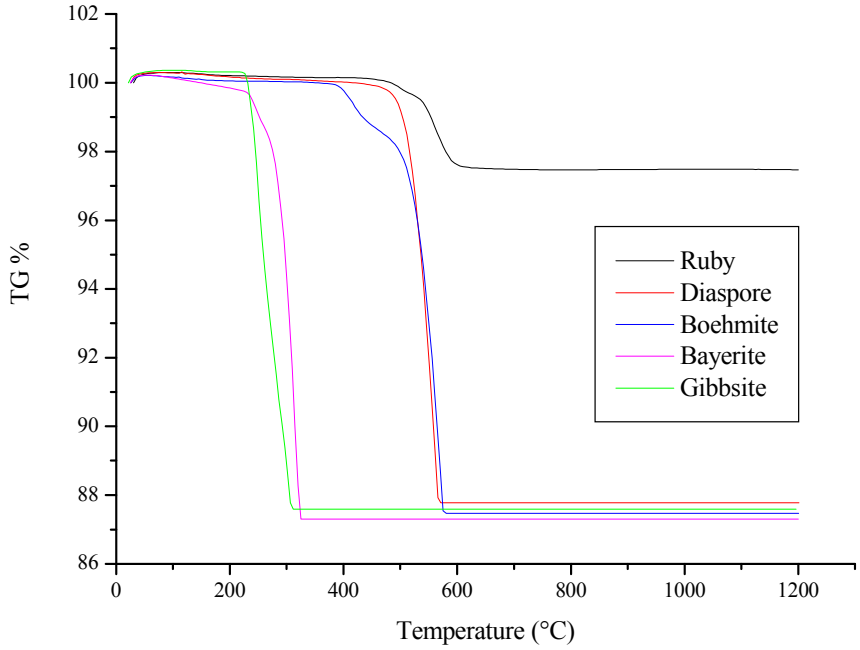

Figure 4.1 Thermogravimetry (TG) diagrams of diaspore, boehmite, bayerite, gibbsite and massive translucent ruby which were annealed up to 1200 °C.

For the DTA results, all of them show endothermic peaks as a result of the absorption of energy (Fig. 4.2). The DTA diagrams can also be separated into two groups (similar to the TG result). The first group contains diaspore and boehmite. Both minerals show the major endothermic band at around 575 °C. On the other hand, diaspore has a minor band at around 125°C while boehmite has the minor bands at around 420°C and 810 °C. In the second group are gibbsite and bayerite. Gibbsite has the major endothermic band at around 355°C and the minor bands at 255°C and 565°C. Bayerite has the major band at around 320°. The minerals in the second group have the major endothermic band at the lower temperature than the first group. These results are to be correlated with the forming temperature of the second group minerals at lower temperature values (see Fig. 1.2)

The TG and DTA results indicate that there were dehydration processes with the heat treatment which can be seen obviously by the loss of weight of the samples and the endothermic bands in the DTA results. Moreover, hydroxide minerals in these experiments

could be separated into two groups by these methods which are correlated with the different crystal structures of each mineral. By the way, diaspore and boehmite are polymorphs of the same chemistry and differ in structural relationships by the packing of the oxygens and hydroxide-anions and also in the same way, gibbsite and bayerite are of similar topology within their same sheet-like structure (Ruan et al., 2001).

The translucent ruby sample core was also heated at the same processes. The TG result show that the sample began to loose weight at around 480 °C, very similar to diaspore and boehmite which ended at around 600 °C. The weight was lost of around 2.5 % by weight. The total amount of weight loss results were ignored in this experiment, because of the high amount of the Al_2O_3 host. The DTA diagram of the ruby sample showed endothermic bands which come up closely to the essential endothermic bands of diaspore and boehmite. The first one was at around 125 °C which may occurr during the burning resulting from impurities such as moisture in the sample. The second one comes at around 420°C which is similar to the minor peak of boehmite. The third band is the major one located at 575 °C. This band lays in the middle between the diaspore and boehmite major bands. The edothermic curve of the ruby may be interpreted as the combination pattern of the two minerals. Thus, the hydroxide mineral which is included in the translucent ruby sample could be diaspore, boehmite or a mixing of both. This result has to be proofed with additional methods like IR-spectroscopy.

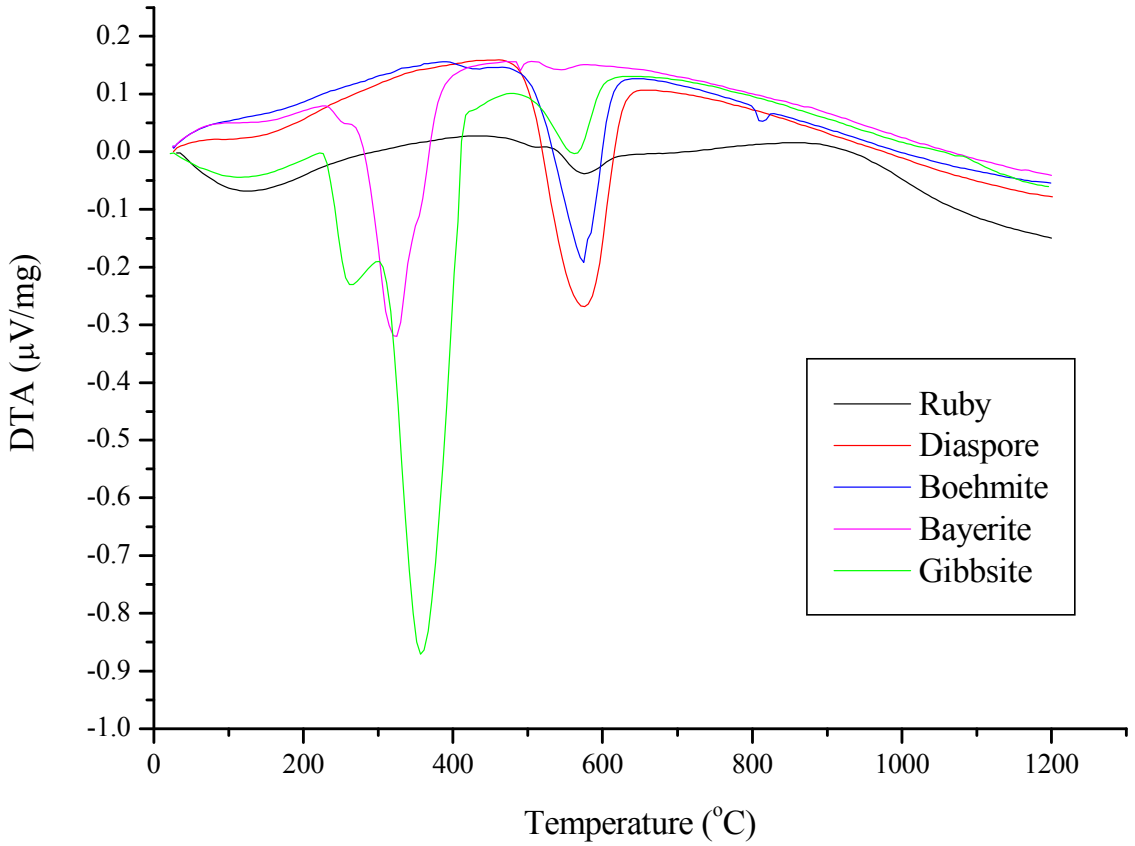

Figure 4.2 Differential thermal analysis (DTA) diagrams of ruby, diaspore, boehmite, bayerite and gibbsite.

5. Radiation-damaged zircon inclusions

5.1 Unheated zircon inclusions

The 25 zircon inclusions in unheated Ilakakan corundums were firstly investigated by Raman spectroscopy to evaluate the degree of metamictization. In this study, the ν_3 Raman band (at around 1000 cm^{-1}) was focused because it is the most sensitive band to estimate the degree of radiation damage to the zircon lattice (Nasdala et al., 1995; Wang et al., 2006). This band shows the highest intensity when the c-axis is 45° to the vibrational direction of the highly polarized laser (around 95%) and disappears when the c-axis is parallel to the vibrational direction of the incident laser beam. However, the orientation of the zircon does not affect the shift of the band position (Wang et al., 2006). Besides, the HfO_2, which is a common minor oxide compound in zircon inclusions in Ilakakan corundum crystals, is not the cause of Raman peak shift (Hoskin et al., 1996, Wang et al., 2006).

Sample No.	Temperature (°C)	ν_3	FWHM (cm^{-1})
Cambodian zircon	unheated	1009.6	2.7
Sri Lankan zircon	unheated	1003.0	9.4
Irradiated zircon	unheated	N.A.	N.A.

Table 5.1 Raman shift and FWHM of free-standing Cambodian and Sri Lankan zircon crystals and the unknown-origin self irradiated zircon.

For the determination of the degree of the radiation-damaged structure parts the FWHM was used. In this study, the degree of radiation-damage of the zircon inclusions were confirmed by composition with the free-standing zircon samples from Cambodia, Sri Lanka, and the highly damaged zircon of unknown origin (Table 5.1; Fig. 3.6). The Raman spectra of these samples were already plotted in Fig. 2.4. The ν_3 band position of Cambodian zircon is at 1009.6 cm^{-1}, which is in the range of crystalline zircon, confirmed by its FWHM of 2.7 cm^{-1}. The band of Sri Lankan zircon is at 1003 cm^{-1} and its FWHM is 9.4 cm^{-1}, which can be identified as belonging to a radiation-damaged zircon. For the highly damaged green zircon,

there are two broad bands, which do not exactly fit the Raman band position and FWHM. This result indicates the amorphous property of this zircon which displays a destruction of the crystalline state by self-irradiation of the host crystal by incorporated radioactive elements itself.

All FWHM values of the unheated zircon inclusions in Ilakaka corundum crystals in this study were between 5.4 and 14.4 cm^{-1} (Fig. 5.1). They were broader than the crystalline zircon, which are therefore in the range of radiation-damaged structures (broader than 3 cm^{-1}; Fig.5.2). Therefore, the FWHM of the zircon inclusions are in between the both free-standing zircon confirming that the unheated zircon inclusions were radiation-damaged zircons.

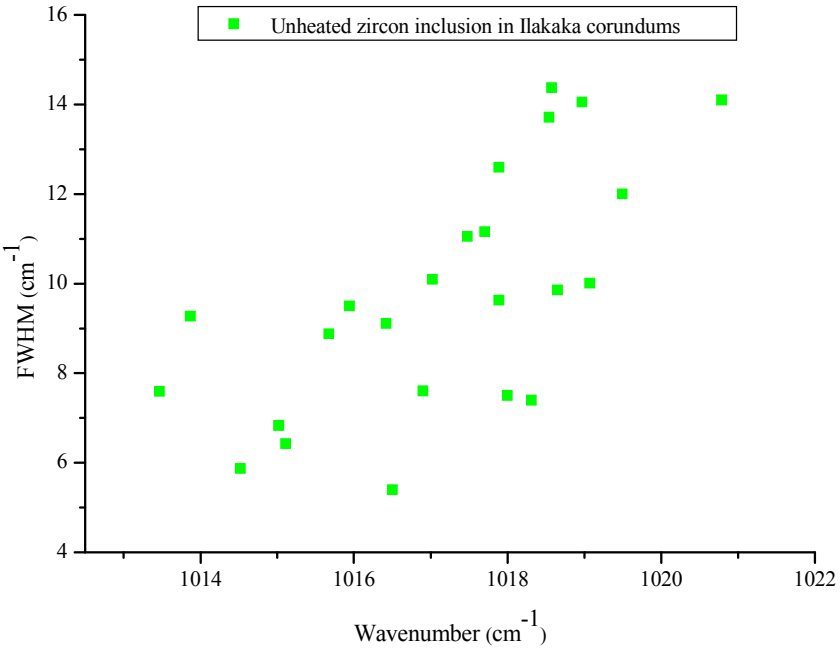

Fig. 5.1 Full-width at half maximum (FWHM) of unheated zircon inclusion of Ilakaka corundum, Raman bands plotted versus band position (Raman shift).

To illustrate the relation between the FWHM and the band position of the ν_3 band, both parameters were plotted in Fig. 5.1. It can be seen that there is an increasing trend of both values. Hence, this indicates that the radiation-damaged degree influences the shift of the

ν_3 band position. The high values of the FWHM affected to the higher shifts of the ν_3 band indicate the destruction of the crystal structure of zircon which is combined with a volume expansion of the inclusion (Harley and Kelly, 2007). For this reason, Wang et al. (2006) calculated an internal pressure around the zircon inclusion in corundum from Ilakaka of about 27 kbar.

Fig. 5.1, shows the variation of the degree of radiation-damage, which mainly depends on the concentration of the radioactive elements (Nasdala et al., 1996). According to this factor, the zircon inclusions in these samples all contain radioactive elements (because the destruction of their crystalline structures is detectable). In this study and in Wang et al. (2006), all of the zircon inclusions from Ilakaka were radiation-damaged zircon objects. However, the zircon inclusions from other origins are not always damaged such as the zircon inclusions in Yen Bai corundum, Vietnam, which has a FWHM at 3.5 cm^{-1} indicating totally crystalline zircon inclusion.

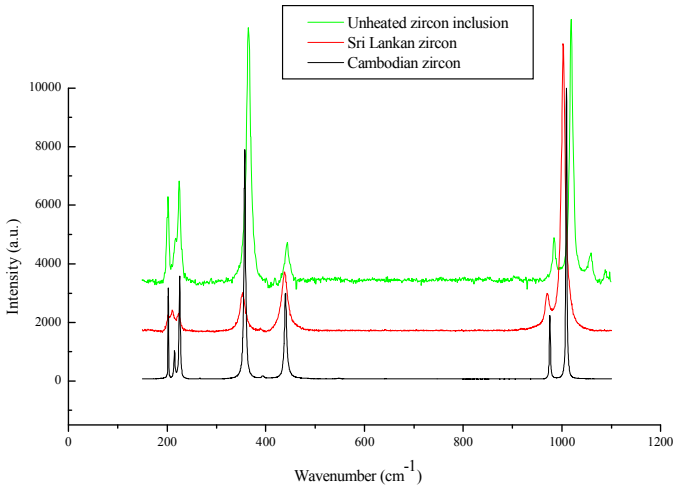

Fig. 5.2 Raman spectra of crystalline zircon from Cambodia (black, FWHM = 2.7 cm^{-1}) compared with a radiation-damaged zircon (red, FWHM = 9.4 cm^{-1}) from Sri Lanka and the unheated radiation-damaged zircon inclusion (green, FWHM = 7.5 cm^{-1}).

The ν_3 Raman band, which is focused on this study, displays the variation of the shift positions due to radiation damage and cooperative properties perfectly (Fig. 5.2). The shift is influenced by many factors, for instance the higher shift due to the increasing pressure (Wang et al., 1993; Knittle and Williams, 1993; Izraeli et al., 1999; Nasdala et al., 2005, Wang et al., 2006) and lower shift due to the disorder of the crystal lattice of the metamictization process (Nasdala et al., 1995; Zhang et al., 2000a).

The critical band position of a crystalline zircon, normally, has the wavenumber at about 1008 cm^{-1} (Zhang et al., 2000b; Wang et al., 2006). For the radiation-damaged zircon, this band shifts to a somewhat lower wavenumber, depending on the degree of radiation-damage. The position of the ν_3 band of a radiation-damaged zircon usually is in the range of 955-1000 cm^{-1} (Nasdala et al., 1995).

The Raman shift can be influenced by another condition such as the pressure as mentioned above. Knittle and Williams (1993) measured the shift of the ν_3 band position in a free-standing crystal under high pressure at room temperature and concluded that the pressure shift of this band is 0.48 cm^{-1} per kbar isobaric pressure. Furthermore, this shift effect was used in the estimation of the trapped pressure between the zircon inclusion and the corundum host by Wang et al. (2006). They reported that the shift of ν_3 band to higher wavenumbers (of the zircon inclusion) indicates the pressure around the zircon inclusion. This effect is counteracting to the above mentioned mechanism which results in a shift of ν_3 band to lower values in free-standing radiation-damaged zircons.

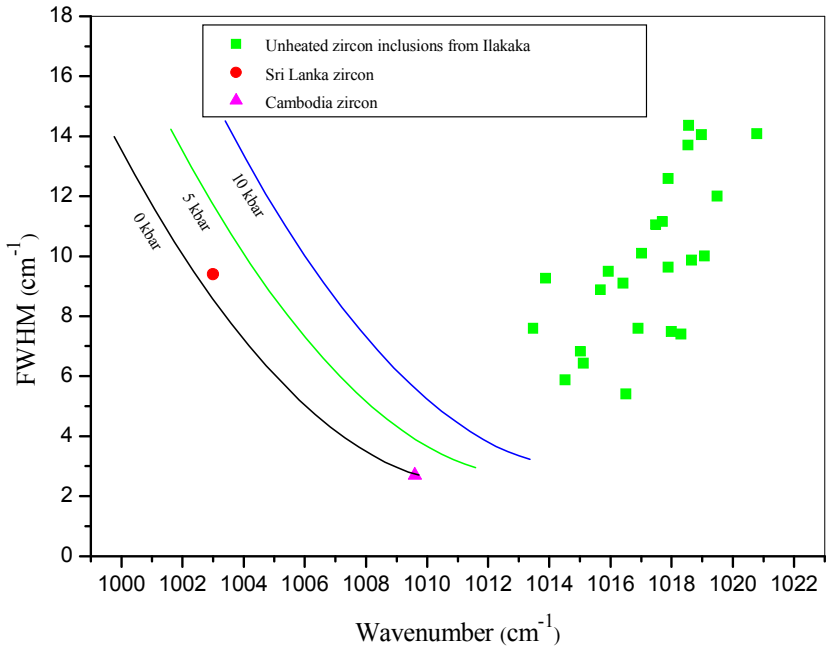

Fig. 5.3 Full-width at half maximum (FWHM) of unheated zircon Raman bands plotted versus band position (Raman shift): data pairs for free standing zircon standards from Cambodia and Sri Lanka, compared with zircon inclusions in corundum from Ilakaka, Madagascar. Additional to that, isobar lines were plotted into the diagram to show the theoretical Raman-shift with increasing pressure.

The zircon inclusions in this investigation, which were under pressure, show totally different results from the free-standing radiation-damaged zircons. Their ν_3 bands in the range of 1013.5 and 1020.8 cm^{-1} and their FWHMs between 5.4 and 14.4 cm^{-1} were plotted in Fig. 5.3, in which the increasing trend of both on Raman shift positions and FWHMs can be observed. The ν_3 bands and the FWHMs of the two reference zircons (Cambodian and Sri Lankan zircons), possessing the different crystallinity, appear in the similar trend of the isobar line reported by Nasdala et al. (2002b) (see the 0-kbar trend in Fig. 5.3; black colour line). Also, even at the higher pressure of 5 kbar and 10 kbar (Fig. 5.3; green and blue colour line, respectively), the isobar line, plotted after the result of Knittle and Williams (1993) appear in the same direction. In contrast, the plotted data of Raman shift positions and FWHMs of zircon inclusions of Ilakakan corundum show nearly an opposite trend to the isobars.

In the heating experiments, three of the zircon inclusions in Cr^{3+} containing green sapphire corundum from Ilakaka (mi7; Fig. 3.4; page 30) were selected for annealing experiments at medium temperature ranges of 500, 800, and 1000°C, respectively, and at a high temperature ranges of 1,200, 1400, 1600, and 1800°C, respectively, for 3 hour per each heating step under normal atmospheric condition. These selected zircon inclusions were observed under the microscope before the heating experiments. They were transparent with a slightly elongate crystal habit with some radial fracture (halo) around them (see Fig. 3.5; page 30) in the host crystal. Their average size is around 50 μm. These inclusions were analysed by Raman spectroscopy and the detailed results are reported in Table 6.2. The Raman band positions of ν_3 of the zircon crystals are in the range of 1018 cm^{-1} to 1016.5 cm^{-1}. The FWHM were between 7.5 cm^{-1} to 5.4 cm^{-1}. These zircon inclusions thus prove to be radiation-damaged zircons and are located in the same trend of the unheated inclusions as the conclusions above (Fig. 5.3).

Sample No.	Temperature (°C)	ν_3	FWHM (cm^{-1})	R_1 Max. Pressure (kbar)
mia7c	unheated	1018.0	7.5	4.8
mia7d	unheated	1016.9	7.6	4.1
mia7e	unheated	1016.5	5.4	3.8

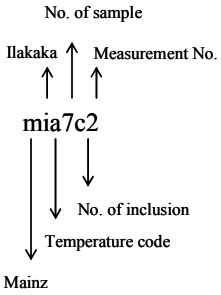

Table 5.2 Raman shift, FWHM, and resulting residual pressure of unheated zircon inclusions in Ilakakan corundum.

These three selected unheated inclusions were analysed with a mapping procedure of the luminescence shift to see the outline of the trapped pressure around the inclusion. The colour-code map showing the shift of the Raman and fluorescence band, used by Nasdala et al. (2005) and Wanthanachaisaeng et al. (2005), was applied in this study. The Lab Spec software converted the shift values to the pressure values (kbar) and plotted them in the colour-code maps (Fig. 5.4). It can be detected that there were trapped pressure values around the inclusion with the maximum value at around 4.8 kbar and the maximum ν_3 band shifts at 1018 cm^{-1} (Table 5.2). In contrast to the reported data of Wang et al. (2006), the maximum pressure in this study at the similar large shift position was much lower than the pressure which was concluded in their report for 27 kbar. This result means that the concluded result of the pressure shift in the free-standing zircon by Knittle and Williams (1993) can not be applied to the shift of the zircon inclusion in the Cr^{3+} containing corundum host. With this pressure values, consequently, the ν_3 Raman band position was obviously impacted and shifted to the higher wavenumber. However, it is difficult to estimate the value of the trapped pressure by the shift of the Raman band because of the heterogeneous metamictization of the zircon (Nasdala et al., 1996).

However, there are also the other conditions, besides the trapped pressure around the inclusion, that cause the large shift of ν_3 Raman bands or affect the zircon Raman shift. At first, it was assumed that the trapped pressure around the inclusion is homogeneous (hydrostatic pressure). But after analyzing the colour-code pressure map, the pressure around the inclusion was found as being distributed heterogeneously (Fig. 5.4). In this case, the anisotropic expansion behaviour of both, inclusion and host, are an important factor. Corundum crystallizes in the hexagonal symmetry that has different thermal coefficients at both principal axis ($a = 7.3 \times 10^{-6}$ and $c = 8.3 \times 10^{-6}$) and zircon in tetragonal has also different coefficients on both ($a = 3.4 \times 10^{-6}$ and $c = 5.6 \times 10^{-6}$) axes. Therefore, the anisotropic

expansion of these minerals could be a cause of nonhydrostatic pressure and also affect the irregular shift of ν_3 Raman band.

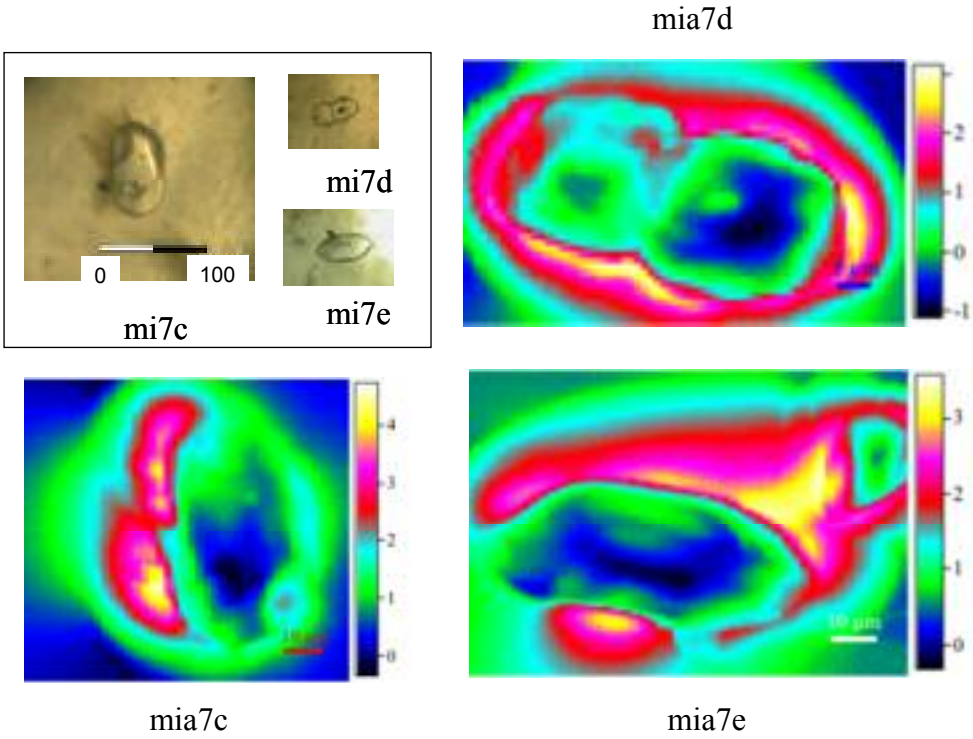

Fig. 5.4 Colour-code maps of pressure values (in kbar) of three unheated zircon inclusions which can be seen in the inset, converted from the shift of Cr^{3+} luminescence.

As it was pointed out earlier, the exact peak position of R_1 and R_2 has been determined with the curve fitting procedure. The function is a combination out of Lorentz and Gauss. In the case of an isotropic pressure distribution, the R_1 and R_2 peak should show a symmetric peak shape (see Ragan et al., 1992). Nevertheless it has been found, that especially close to the inclusions, an asymmetric component was observed. In Figure 5.5, the FWHMs of about 30,000 accumulated spectra of R_1 around the zircon inclusion with Raman mapping of unheated corundum show not only the width variation of the peaks at the same pressure value but also the broadened peak values due to the higher pressure values. These results also indicate that the pressure around the inclusion is not hydrostatic pressure, the asymmetric

component could be explained by the high pressure gradient towards the inclusion (see Eggert et al., 1989).

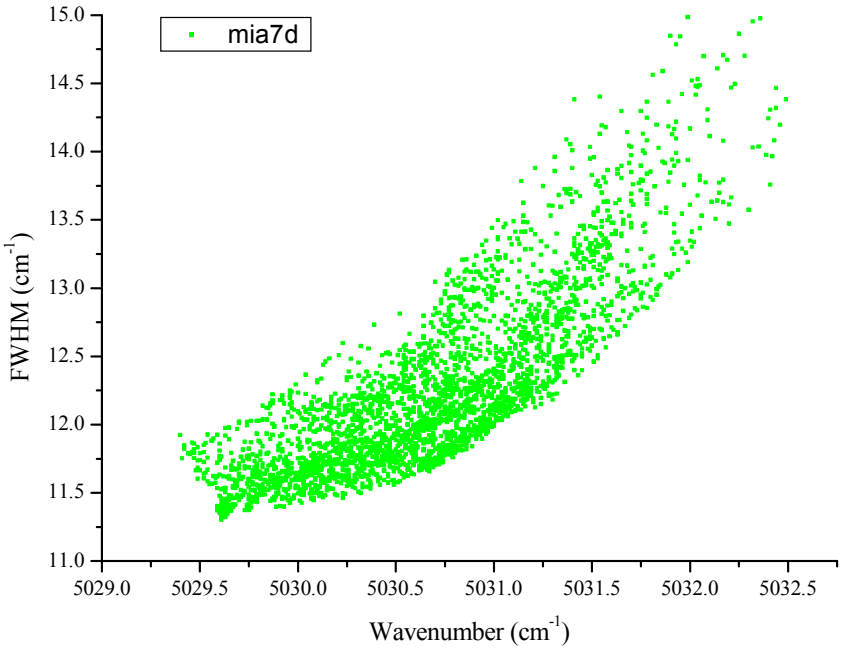

Fig. 5.5 Fluorescence data of R_1 peak mapping of an unheated corundum crystal with zircon inclusion (mia7d). These data were accumulated from about 30,000 spectra around the zircon inclusion showing the broadened peak and the peak shift due to the pressure gradients.

5.2 Medium temperature treatment of corundum with zircon inclusions

5.2a Recrystallization of unheated zircon inclusions

The heating experiment at the medium temperature range was done with the green sapphire corundum bearing the zircon inclusions. These zircon inclusions were observed under the microscope after being heated. They did not show any differences from the unheated state. Their Raman results are demonstrated in Table 6.3 and are plotted in Fig. 5.6, correlating the ν_3 band positions and the FWHMs, and correlating the FWHMs and temperature values in Fig. 5.7. It can be seen that the FWHMs decrease firstly after annealing at 500°C. The shift to lower values of this band can be seen but it is not very significant, at this annealing temperature in combination with the given pressure, however, the small decreasing of the FWHMs can be considered as an evidence of the beginning of the recrystallization of the radiation-damaged zircon inclusions, which is similar to the result of Zhang et al. (2000b). They reported that the structure of the damaged free-standing zircon recovered after annealing at a temperature as low as around 426°C. It can be concluded that, however, the results in this study received from the annealing at 500°C for 3 hour do not deliver significant change.

In further rising the temperature to 800°C, the decrease of FWHM shows that the highest value changes from 7.5 cm^{-1} to 5 cm^{-1} (Fig. 5.8). The lowest FWHM at this temperature is 4.4 cm^{-1}, close to the FWHM of the fully crystalline zircon. The Raman shift obviously shows the decrease to the lower wavenumber at 1014.3 cm^{-1}. With this result, it can be concluded that the radiation-damaged zircon inclusions have recrystallized partially at this temperature in combination with the chosen heating parameters and the given pressure. This result is similar to Zhang et al., (2000b) where the zircon free-standing has partially recrystallized near 726°C involving epitaxial growth.

Sample No.	Temperature (°C)	ν_3	FWHM (cm^{-1})	R_1 Max. Pressure (kbar)
mia7c	unheated	1018.0	7.5	4.8
mib7c2	500	1018.0	7.0	5.0
mic7c1	800	1014.3	5.0	3.6
mid7c1	1000	1013.2	3.4	2.4
mie7c	1200	1013.2	3.1	2.9
mif7c1	1400	1017.7	3.0	2.8
mig7c6	1600	1019.8	2.9	4.5
mih7c	1800	monoclinic ZrO_2+SiO_2 glass		8.1
mia7d	unheated	1016.9	7.6	4.1
mib7d2	500	1016.6	7.3	3.0
mic7d1	800	1015.6	6.1	2.2
mid7d1	1000	1013.5	3.7	1.6
mie7d	1200	1013.8	3.7	2.3
mif7d2	1400	1018.4	2.9	2.4
mig7d1	1600	1019.9	3.0	3.1
mih7d	1800	monoclinic ZrO_2+SiO_2 glass		5.4
mia7e	unheated	1016.5	5.4	3.8
mib7e1	500	1015.6	5.3	4.7
mic7e1	800	1013.9	4.4	2.9
mid7e1	1000	1013.5	3.0	1.9
mie7e	1200	1013.6	3.0	2.7
mif7e3	1400	1018.1	2.9	2.8
mig7e1	1600	1021.4	2.8	3.7
mih7e	1800	monoclinic ZrO_2+SiO_2 glass		2.4

Table 5.3 Raman shift, FWHM, and resulting residual pressure between zircon inclusions in Ilakakan corundum before and after annealing at each target temperature.

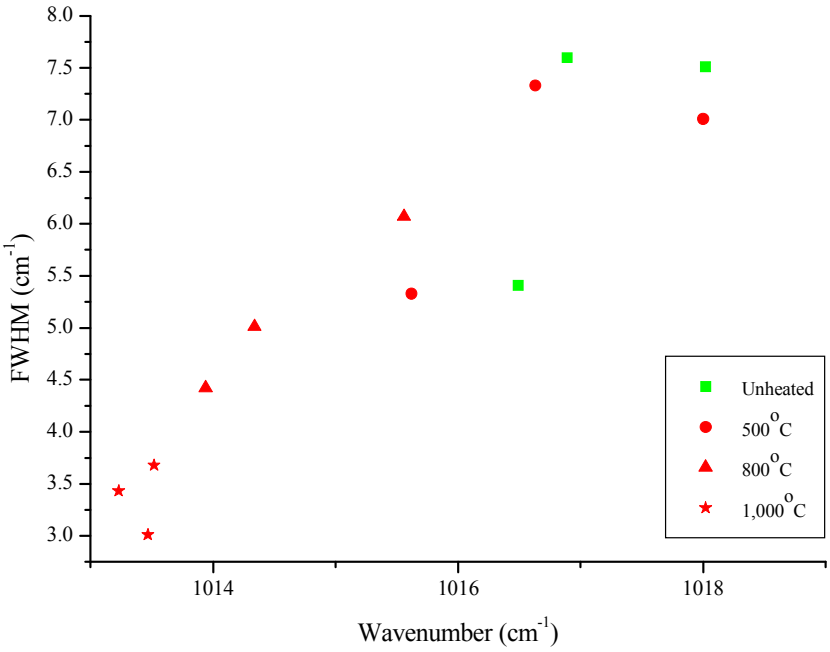

Fig 5.6 Plot of FWHMs versus Raman shift positions of the ν_3 Raman bands of three zircon inclusions after being heat-treated at medium temperatures (500, 800, and 1000°C).

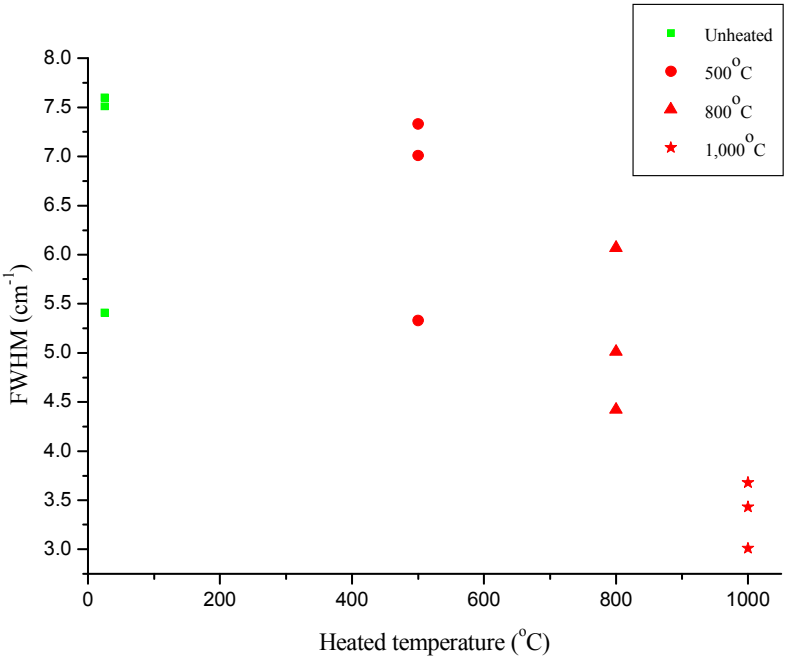

Fig. 5.7 Full width at half-maximum (FWHM) vs. the sample heating temperature show the decrease of the FWHM at each step of the heat treatment. This decrease was influenced by the recrystallization of the zircon inclusion.

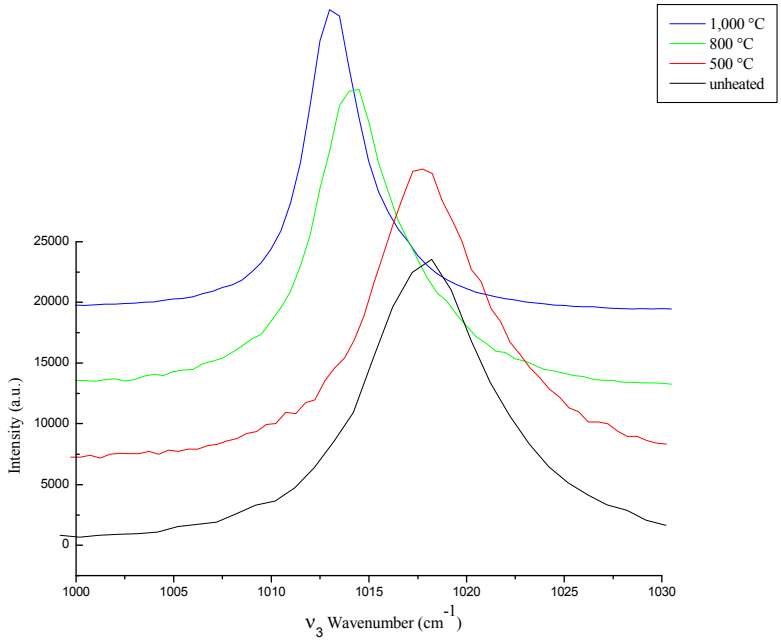

Fig. 5.8 Shift of the ν_3 Raman band (and the obvious change of FWHM) of the zircon inclusion after medium annealing temperatures.

After annealing at 1000°C, the FWHM values of the inclusions decrease close to the value of crystalline zircon, which is around 3 cm^{-1} and the Raman shift continues to decline to the lowest wavenumber at 1013.2 cm^{-1}. This result was supported by the conclusion of Nasdala et al. (2002a) that the free-standing zircon recovered to well-crystallised $ZrSiO_4$ at around 1100°C.

In figure 5.6, the results of the Raman shift values and of the FWHMs for the ν_3 band were plotted illustrating the linear trend, decreasing from high wavenumbers of the Raman shift and broad FWHM to the lower wavenumbers and the narrower FWHM. This trend shows that the position of the bands shift to the lower position when the radiation-damaged zircon recrystallizes due to the heat treatment. As described above, the FWHM of the crystalline zircon is approximately 2 cm^{-1}, which is close to the FWHM result at 1000°C. Moreover, the trend show the step of recrystallization from radiation-damaged zircon to partially crystallized until fully recrystallized zircon in this temperature range to be

comparable with the results of Özkan (1976), Capitani et al. (2000), Zhang et al. (2000b), Nasdala et al. (2002a), and Geisler (2002). Besides, this recrystallization also influences the shift of the ν_3 band to the lower wavenumber, which will be discussed further. Therefore, the radiation-damaged zircon inclusions can recrystallize to the well-crystalline ones by heat treatment at this medium temperature range.

The radiation-damaged zircon inclusions in this study have almost fully recovered at this annealing temperature and ambient pressure. The changing of the FWHMs can be interpreted obviously and such values are not found in the unheated Ilakaka corundum. With this result, it can be concluded that the measurement of FWHMs of radiation-damaged inclusion zircon crystals may be applied for the identification of any heat treatment history of gem corundum crystals from Ilakaka, Madagascar.

5.2b Pressure development between host and guest during heat treatment

To investigate the cause of the ν_3 band shift to lower wavenumber after heating at the medium temperature range, the determination of the trapped pressure by the R_1 luminescence shift was carried out again. The three heated inclusions were mapped and plotted in the colour-code mapping method to show the distribution of the pressure around the inclusion, comparing this with the position shifts of the bands (Fig. 5.9). The colour-code maps of the inclusions exhibit the decrease of the trapped pressure at each step of heating. The results between the shift of ν_3 band and the trapped pressure around the inclusion from the colour-code maps are plotted in Fig. 5.10 to show the relationship between them.

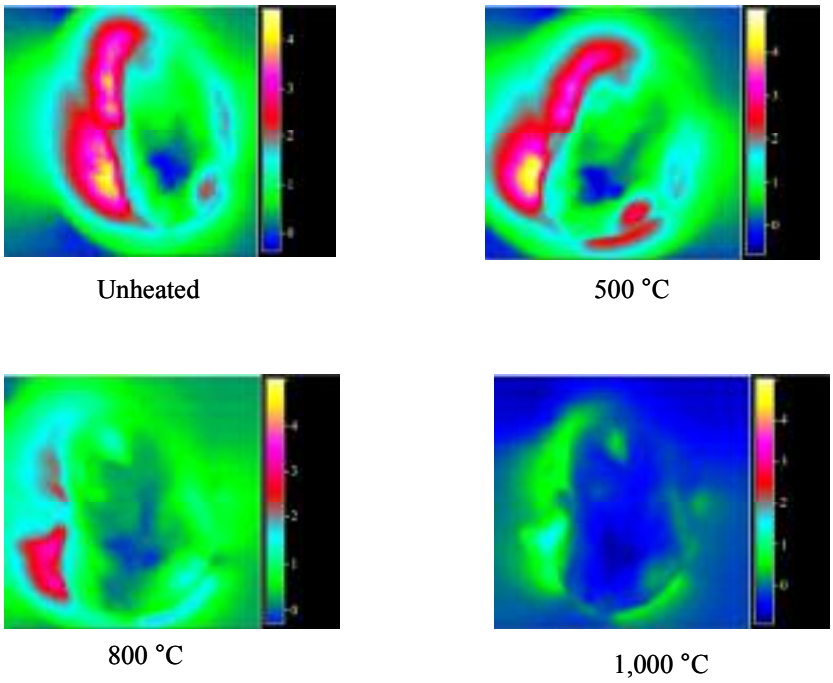

Fig. 5.9 Colour-code maps of the unheated, radiation-damaged zircon inclusion and the heated inclusion at 500, 800 and 1000°C. It shows the decrease of the trapped pressure between the inclusion and the corundum host with increasing temperature.

In Fig. 5.10, the maximum trapped pressure of the unheated radiation-damaged zircon can be evaluated at 4.8 kbar and the ν_3 band position is 1018 cm^{-1} (sample 1 of 3). After being heated at 500°C, there is a small change of both values but they are not significant. The change of the Raman band position can be seen after heat treatment at 800°C. The ν_3 band position for sample 1 of 3 relocates to 1014.3 cm^{-1} and the pressure decreases to 3.6 kbar. The decreasing of both values was also found after heating at 1000°C. They are at 1013.2 cm^{-1} and 2.4 kbar, respectively. The two other inclusions sample behave similarly. At this medium temperature range, the linear trend of decreasing displays the relationship between the recrystallization, the pressure, and the Raman shift of the radiation-damaged zircon. As a consequence, the shifting of the Raman band can be explained by the change of the zircon inclusion´s crystallinity and therefore its volume. These results reveal the decrease of the trapped pressure and the influence to the shift of the Raman bands to the lower position in the recrystalline- zircon inclusion. Therefore, it can be concluded that the ν_3 band position and the

trapped pressure have a linear correlation with the crystallinity of the zircon inclusion in the medium-temperature heat treatment. But nevertheless, if we extrapolate this linear trend to 0 kbar pressure the Raman band position is about 1010 cm^{-1}. However, comparing with a free standing crystalline zircon, it should have a ν_3 band position at 1008 cm^{-1}. This small difference shift could also be explained by the nonhydrostatic and isobaric pressure distribution around the inclusion.

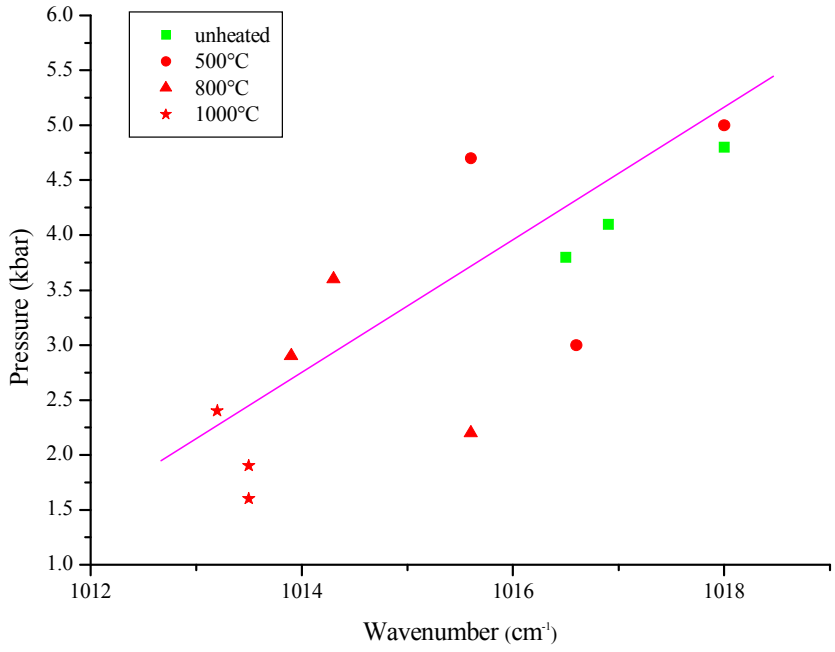

Fig. 5.10 Maximum pressure of the host corundum in close proximity to zircon inclusions plotted versus the spectral position of the corresponding ν_3 Raman band of zircon (three samples). Note the pressure changes as caused by the heat treatment at 500, 800, 900, and 1000°C. The pink line shows the decreasing linear trend of the pressure and the ν_3 band position between 500 to 1000°C because of the recrystallization of the zircon inclusion.

5.3 High temperature heat treated zircon inclusions

The same corundum host sample has further been heated at the higher temperatures of 1200, 1400, 1600, and 1800°C. Under the microscope, it can be observed that the surface of the zircon inclusions firstly changes to a frosted-like surface at 1400 °C (Fig. 5.11). The halos, fractures around the inclusions, were also healed at this temperature. The reaction of the surface of the zircon inclusion during the high-temperature heat treatment was also reported by Wang et al. (2006). They concluded that the reaction of the $ZrSiO_4$ (solid) to ZrO_2 (solid) and SiO_2 (solid) begins at the temperature as low as 1400°C and results in a frosted-like surface of the inclusions. This transformation on the surface of zircon inclusions takes place more obvious at higher temperatures. The frosty appearance was clearly seen at 1600°C in this study. It stems from the decomposing reaction at the surface, which is a interface between host and inclusion, which gave more ZrO_2 and SiO_2 phases, compared to the treatment at 1400°C. All zircon inclusions in this experiment melted during heating at 1800°C. They lost their crystal surface and became irregular in the outline, caused by the melting of both, themselves and the surrounding host. Thus, as the conclusion, the beginning of the phase transformation of zircon inclusions can be seen under the microscope after the heating at 1400°C. The zircon inclusions melted completely and transformed into other phases after annealing at 1800°C. These results will be confirmed by Raman spectroscopy and scanning electron microscope in the next step.

The FWHM values of ν_3 for zircon after heating at 1200°C, (already recrystallized at 1000°C), do not show any significant changes; values were at around 3 cm^{-1} (Table 5.3; Fig. 5.12). The FWHM value changes resulting after heating temperatures of 1400°C and 1600°C were similar to those at 1200°C, which supports the indication of the crystalline zircon phase (well-crystallized zircon can be stable up to 1690°C at ambient pressure, Nasdala et al., 2003). However, the increase of the trapped pressure and the change of the Raman band position

after this temperature, which will be discussed thoroughly in the next part, can be observed (Fig. 5.13).

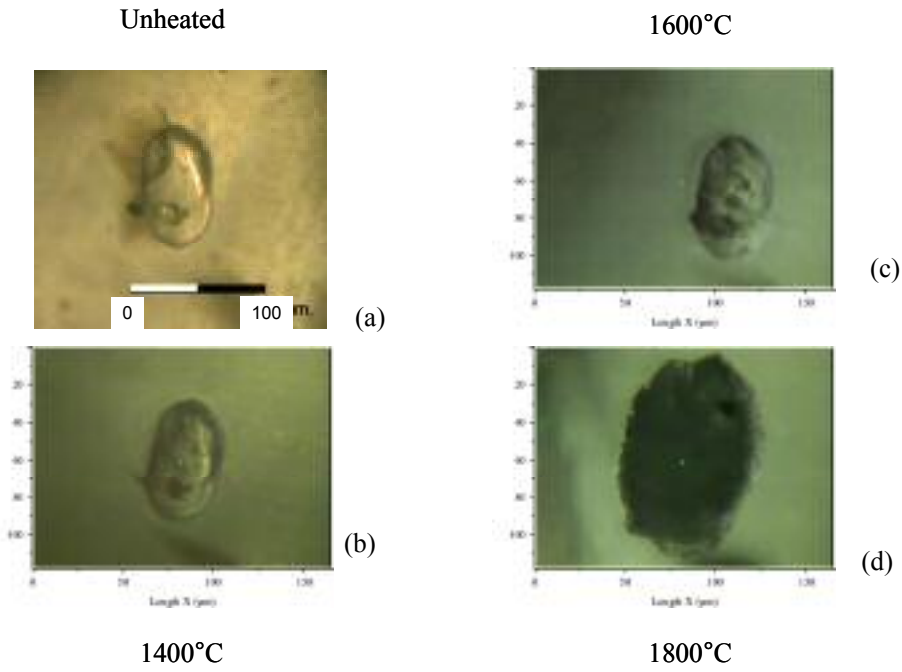

Fig. 5.11 Microscopic observation of the unheated radiation-damaged zircon inclusion (a), compared with the heated zircon inclusion at 1400 (b), 1600 and 1800°C, respectively. The surface change (frosted) and the healed halo began at 1400°C and can obviously be detected at 1600°C (c). The inclusions reacted to multi-phase m-ZrO_2 and a SiO_2-rich phase after being heated at 1800°C (d).

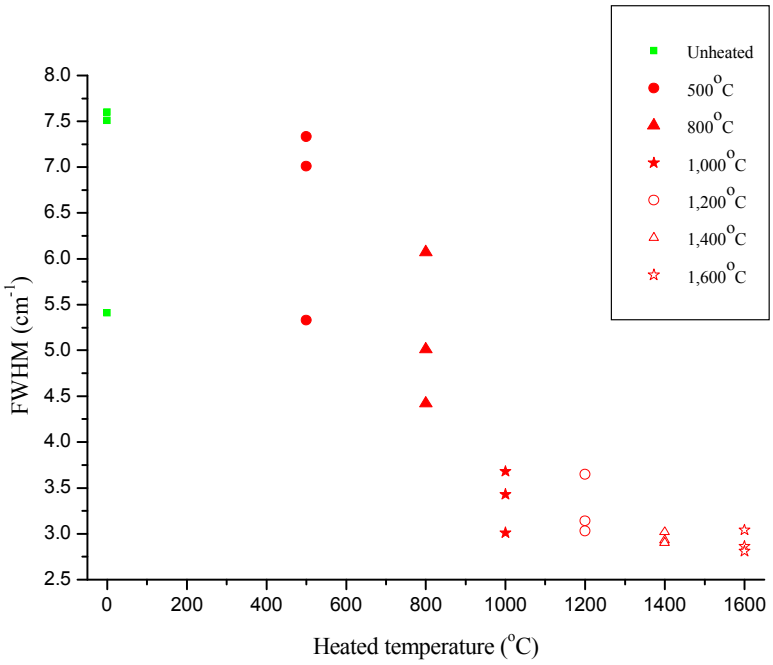

Fig. 5.12 FWHM vs. zircon heating temperatures.

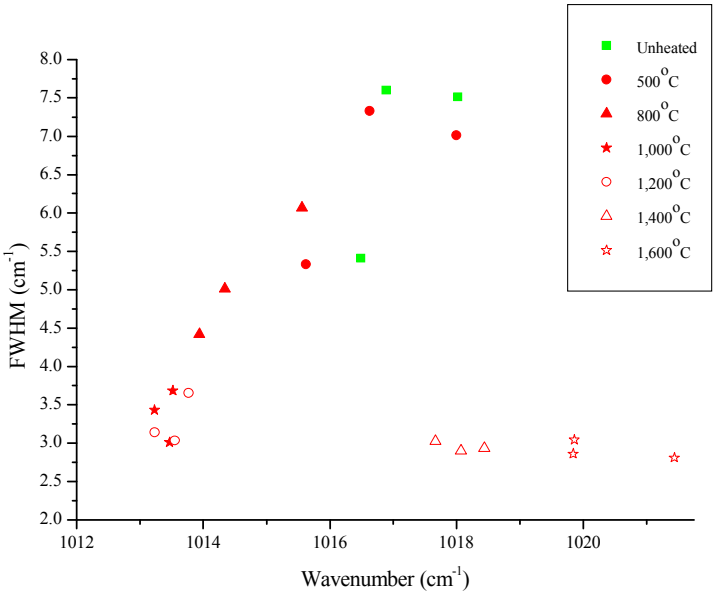

Fig 5.13 Plot of FWHMs versus Raman shift positions of the ν_3 Raman bands of three zircon inclusions after being heat-treated at different temperatures (500, 800, 1000, 1200, 1400, and 1600°C).

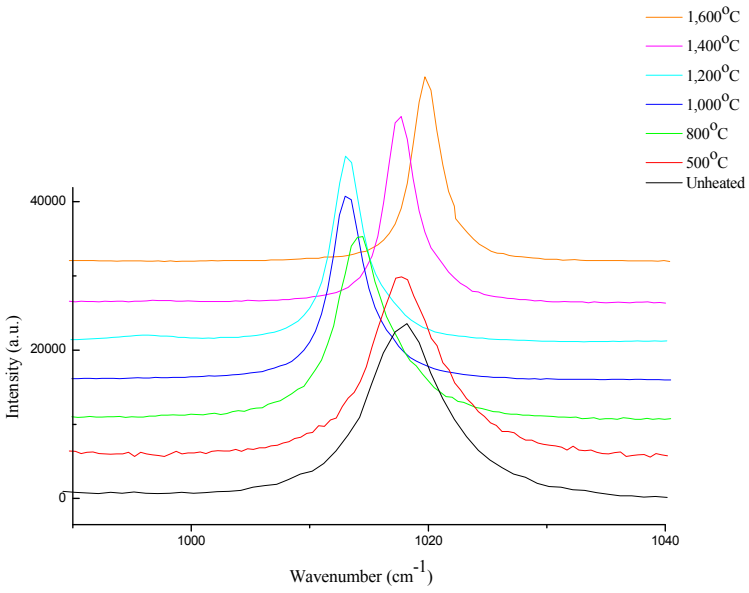

Fig. 5.14 Shift of the ν_3 Raman band of the zircon inclusion at several annealing temperatures. FWHM values are obviously decreasing with increasing temperature.

After heat treatment at the high temperature values, compared with the lower temperature range, different results of the Raman band positions and related internal pressures were found. The ν_3 band position of the zircon after being heated at 1200°C still show the similar values(around 1013 cm^{-1}) as at 1000°C (Fig. 5.14) but the calculated pressure at this temperature (1200°C) increases from 2.4 to 2.9 kbar (see Table 5.3; Fig. 5.15). Conversely, at 1400°C, the Raman shift increases obviously from 1013.2 to 1017.7 cm^{-1}, but the pressure still remains similar to the value gained at the 1200°C. Furthermore, at 1600°C, both Raman shift and pressure increase to 1017.7 cm^{-1} and 4.5 kbar.

Although the pressure around the inclusion and the FWHM values gradually decrease to the minimum value of the crystalline zircon under the temperature from 500°C until 1000 °C with a linear trend, in contrast, the pressure continuously increases to higher values for temperatures from 1200°C to 1600 °C at an exponential rate, while the FWHMs are not significantly changed (Fig. 5.17). From this result, it can be concluded that, under the heating temperatures from 1200°C to 1600 °C, the FWHM, belonging to the highly ordered zircon, is not affected by the increase of pressure, indicated by the Raman shift of the ν_3 band.

According to the pressure increase after being heated at high temperatures, the mapping method of the ν_3 band shift was applied to the zircon inclusion (mi7d) after being heating at 1600°C (Fig. 5.18). Observed under the microscope, the inclusion shows the alteration of the surface as to be frosted-like because of mineral reaction due to the heat treatment. The result of the Raman shift in the map demonstrated also the phase change at the rim of the zircon inclusion, which was the transformation of $ZrSiO_4$ into m-ZrO_2 and a SiO_2-rich phase. The Raman and fluorescence peaks of the m-ZrO_2 phase replace the zircon Raman peaks in this area which is a similar result to Carlone (1992); Zhang et al. (2000a); Rankin and Edwards (2003). This result was also reported by Wang et al. (2006) who stated that the decomposition reaction was mostly limited to the rim of the inclusion. During this increasing pressure, however, there is not only the occurrence of phase transformations but also the

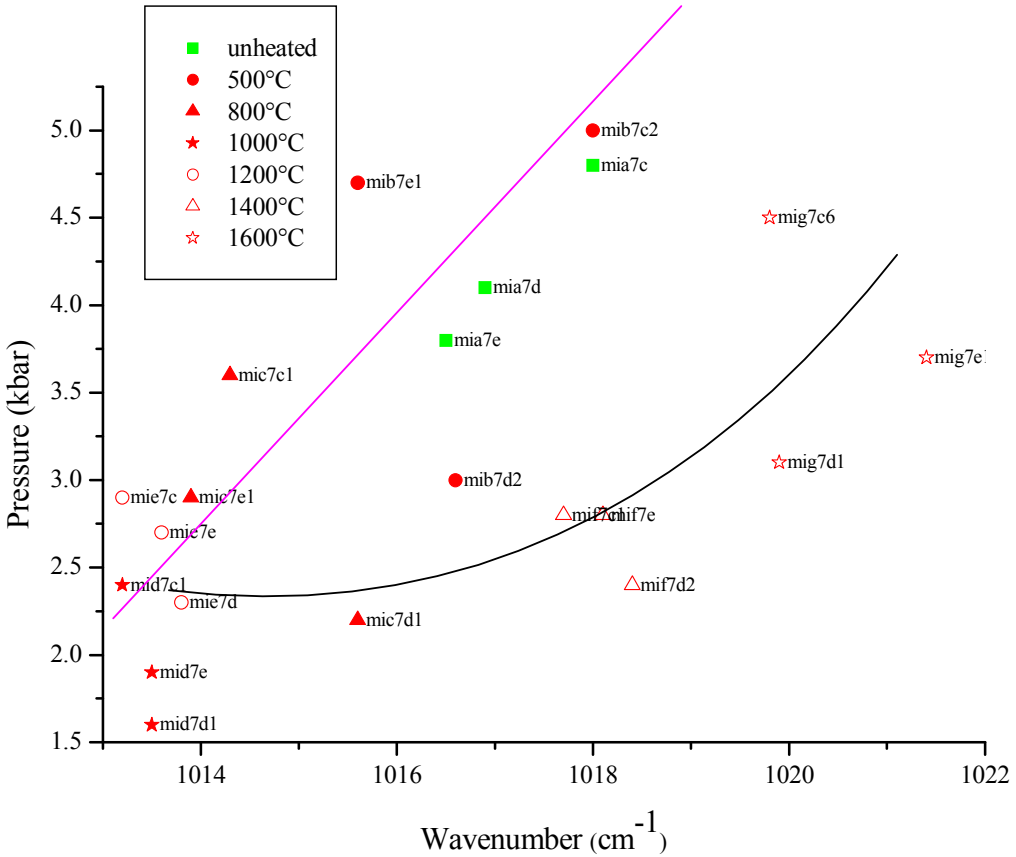

Fig. 5.15 Calculated maximum pressure of the host corundum in close proximity to zircon inclusions plotted versus the spectral position of the corresponding ν_3 Raman band of zircon (three samples). Note the pressure changes as caused by the heat treatment at 500, 800, 1000, 1200, 1400, and 1600 °C. The pink line shows the decreasing linear trend of the pressure and the ν_3 band position between 500 to 1000°C because of the recrystallization of the zircon inclusion. The black line shows the increasing pressure / wanvenumber ratio at an exponential rate from 1200 to 1600°C because of the volume expansion of the phase change in the inclusions.

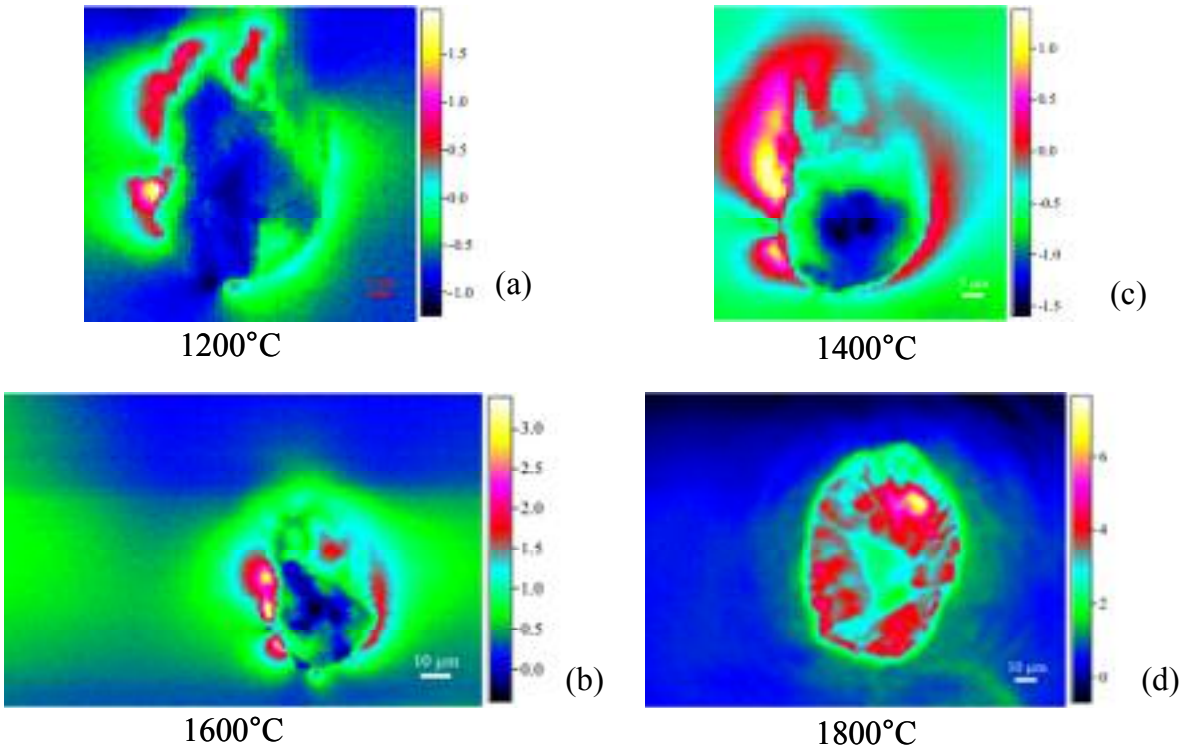

Fig. 5.16 Colour-code maps of the pressure distribution in the corundum host, produced by the zircon inclusions at 1200, 1400, 1600 and 1800°C. They show the increase of the trapped pressure after the high-temperature heat treatment. At 1800°C (d), it can be seen that the concentration of the highest pressure nearly centred inclusion (differential scales).

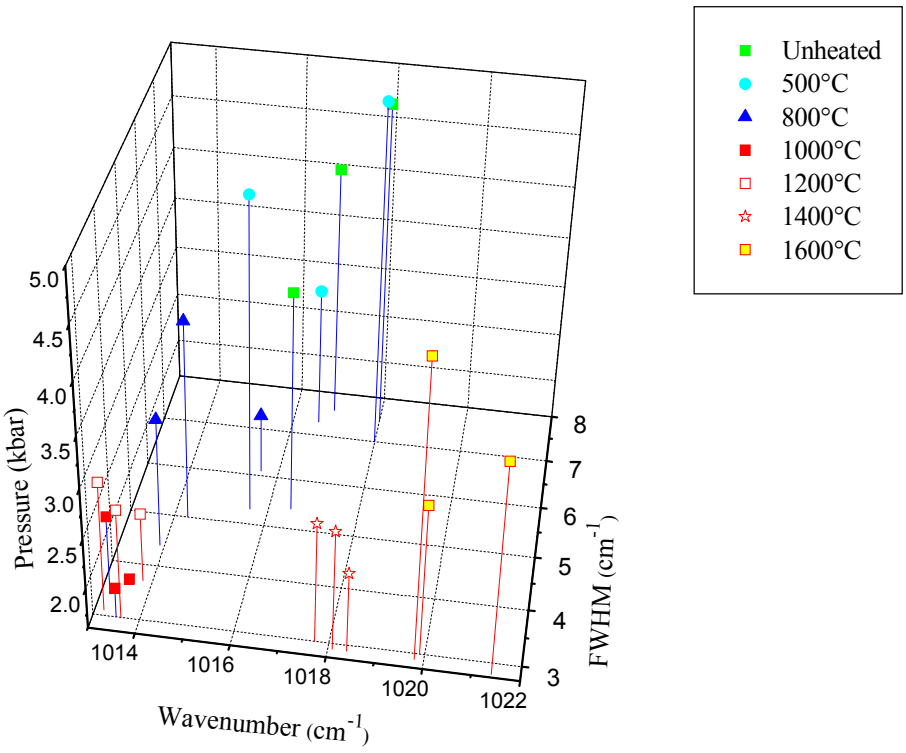

Fig. 5.17 Three-dimensional plot of the ν_3 Raman band position, FWHM and trapped pressure of the selected inclusion(s) in this experiment.

expansion of the volume due to the newly transformed phases, especially the obviously large volume expansion of the SiO_2-rich phase. This decomposition of the zircon inclusion causes the expansion in its volume expressed by the higher stress around the inclusion. Therefore, this is one explanation for the higher shift of the Raman position and the increase of the pressure after being annealed at the high temperature range.

Wang et al. (2006) have reported that the inclusion was transformed into ZrO_2 phase and SiO_2 phase after heating above 1680°C. They also reported the FWHM values before and after heating. The values given by Wang et al. (2006), at every heating temperature, are broader (around 8.5 cm^{-1}) than the result in this study. This dissimilar result is probably because of the resolution difference of the Raman spectroscopy or differences in the heating or cooling process and/or the effects of the annealing time, impacting to the width of FWHM values.

Therefore, in conclusion, it can possibly be declared that, at 1200°C, the decomposition occurred only at the outer rim of the inclusion and did not impact on the whole volume of the zircon inclusion. But, after being heated at 1400°C, more progress of the decomposition has taken place, and then the volume expansion of this decomposition increases enough to affect the stress in the lattice of the zircon inclusion. This stress impacted the shift of the Raman band position to the higher position.

Another explanation of the increasing stress might be the cooling rate of the sample after being heated. Especially the cooling rate from high temperature (1200°C to 1800°C) is much faster as the cooling rate from medium temperatures (500°C to 1000°C). Groß, et al. (1998) reported that the residual stress increases linearly during cooling the α-Al_2O_3 to the room temperature. Therefore, this could lead to an additional stress around the inclusion and could also explain the high crystallinity in combination with the higher Raman shift and higher internal pressure around the inclusion. Furthermore, after heating at 1800°C, the Raman bands of zircon inclusions disappear because of the melting.

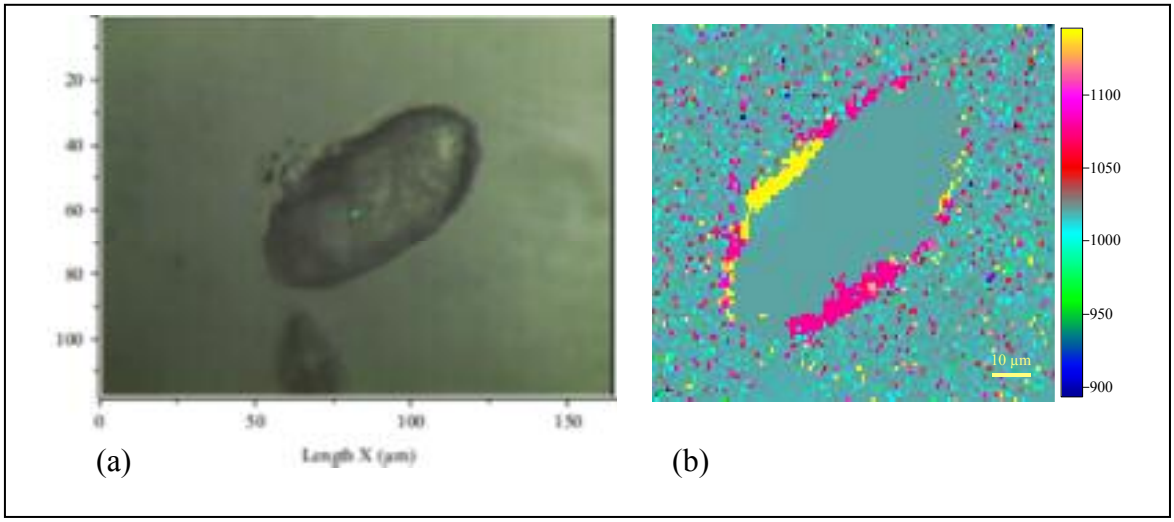

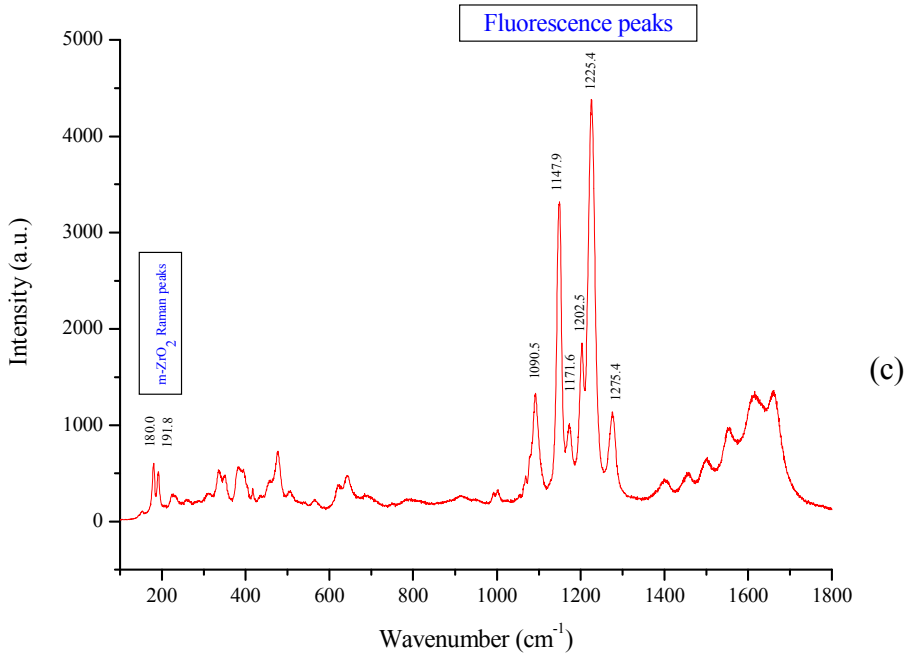

Fig. 5.18 The left picture is a heat treated inclusion with frosted surface. The sample was annealed at 1600°C. On the right side is the Raman map of the inclusion shown on the left side (a). Blue green colour in the Raman map (b) represents the corundum host. Yellow and reddish purple colours show the area of m-ZrO_2, which has transformed from $ZrSiO_4$ and which can be seen in the spectrum below (c). Note, however, that the most intense bands are NOT Raman bands but are luminescence emissions (most probably emission centres related to rare earth elements in monoclinic zirconia) that overlay and partially obscure the Raman spectrum.

5.4 Melting inclusions

The final experiment of the heated zircon inclusions is the heat treatment at 1800°C, which is close to the melting point of corundum (2050°C). The microscopic observation after heating has been shown the molten inclusions (Fig. 5.19). The outline of the inclusions was changed because of the melting of themselves. The crystal face and distinct interface with the host corundum has totally disappeared, there is no more phase boundary. Some of these inclusions showed the leaked of the melt intruding into the cracks of the corundum host around the former inclusion (Fig. 5.20). Some molten inclusions decomposed and show melt aureoles, drip-like trails, and discoid fractures (Fig. 5.21).

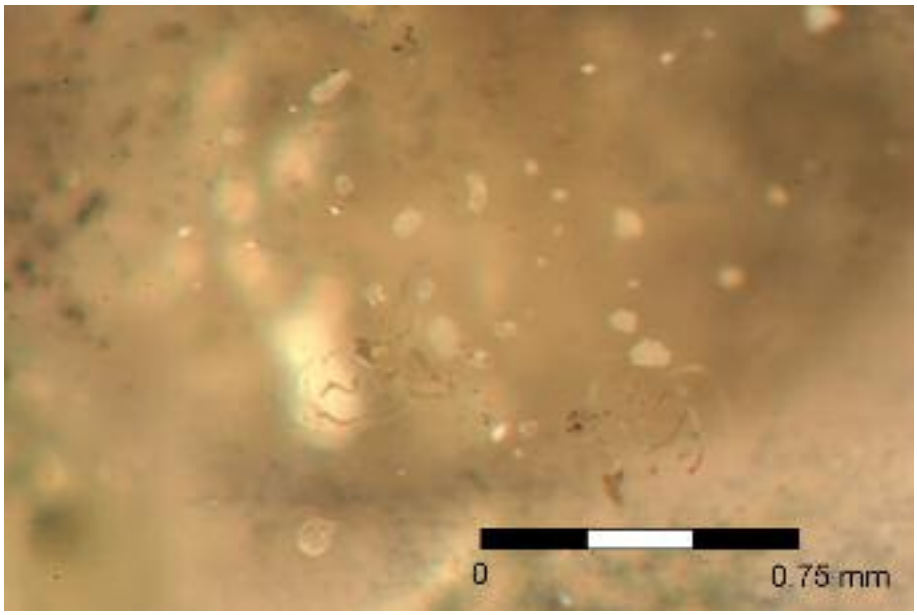

Fig. 5.19 Molten zircon inclusions in Ilakakan corundum after heating at 1800°C. The inclusions are transformed to irregular forms with white colour (snow ball) and some of the melt droplets show aureoles, drip-like trails, and discoid fractures.

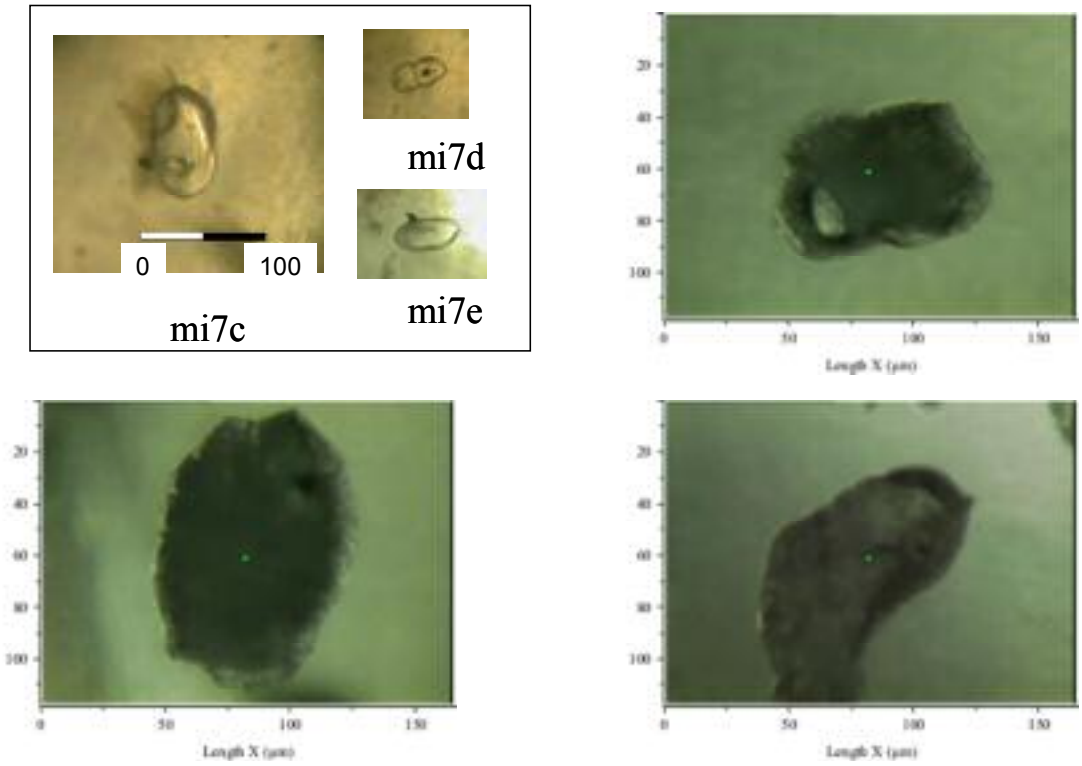

Fig. 5.20 The melting process of the three selected zircon inclusions in the corundum host crystal after being heated at 1800°C. The inclusions have lost the original features and are transformed from zircons to other phases: m-ZrO_2 and SiO_2-rich phases. The picture below right shows the molten inclusion within fracture due to the expansion of the process of transformation. The inset shows the original unheated inclusions.

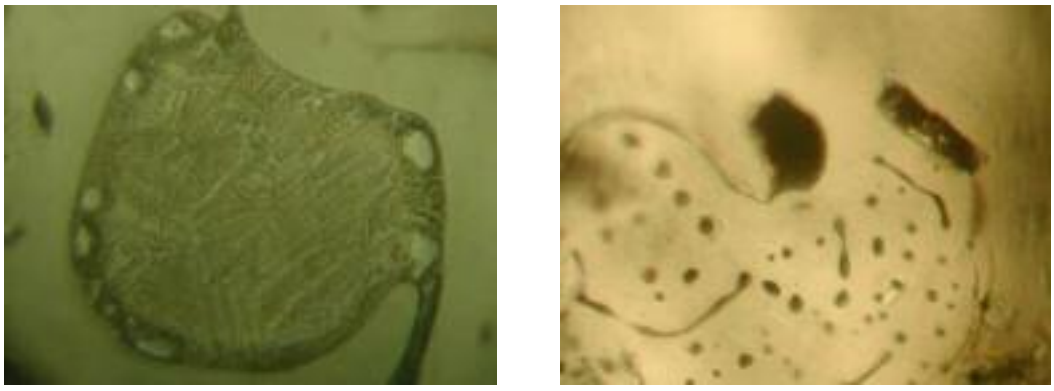

Fig. 5.21 Micro-photographs of former zircon inclusions. Heat-treatment at 1800 °C is the cause of melting and, thus, disappearance of inclusions.

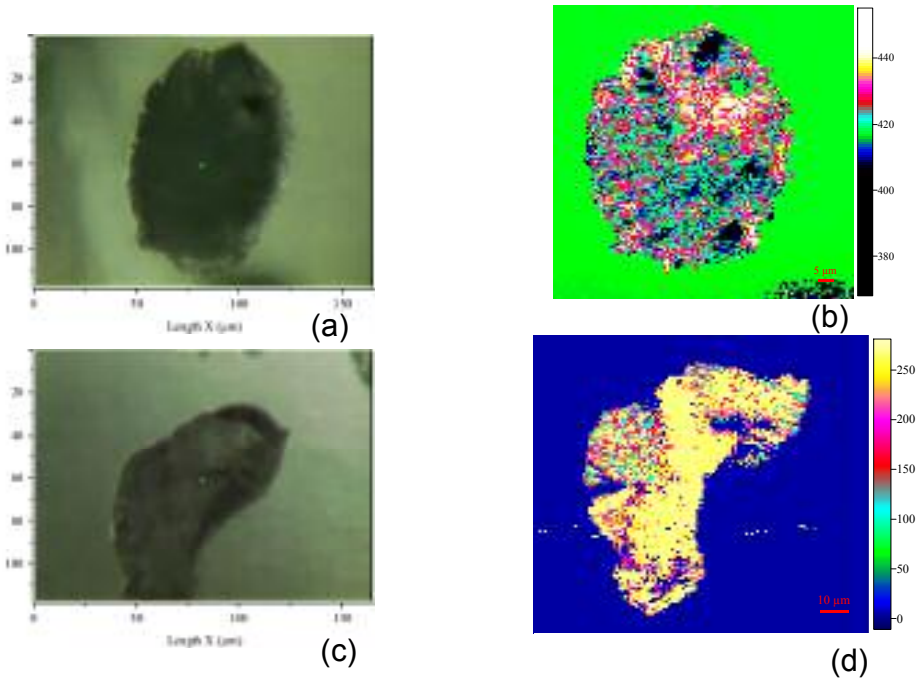

Fig. 5.22 Molten zircon inclusion and its Raman maps consisting of the m-ZrO_2 and SiO_2-rich phase after heating at 1800°C. (a) The molten inclusion with no fracture. (b) The Raman map of (a) shows the m-ZrO_2 and SiO_2-rich phase (various colours) in the host corundum (green colour). (c) The molten inclusion with fracture. (d) The Raman map of (c) shows the m-ZrO_2 and SiO_2-rich phase (various colours) and the host corundum (blue colour). It can be seen the leakly of the m-ZrO_2 and SiO_2-rich phase along the fracture can be seen.

As a result of interpreting Raman spectroscopical data, it may be stated that the ν_3 Raman bands disappear at this temperature and were substituted entirely by the Raman and fluorescence spectrum of m-ZrO_2 (Fig. 5.18). Rankin and Edwards (2003) and Wang et al. (2006) concluded that the zircon inclusion at first decomposes, then melts at high temperature and has been replaced by the m-ZrO_2 phase and SiO_2-rich phase. In this study, the zircon inclusions were totally transformed into other phases which can be seen in the Raman maps of the heated inclusion at 1800°C (Fig. 6.22). In Fig. 5.22 (b) and (d), the Raman maps show the various colours in the inclusion, outline in both maps, represent the m-ZrO_2 and SiO_2-rich phase and the green and blue colours represent the host corundum In addition, it can be seen the intrusion of the m-ZrO_2 and SiO_2-rich phase into the fracture of the host corundum ((d) in Fig. 5.22). Moreover, the irregular surface of the molten inclusion can be observed by this Raman map because the corundum has been found at the

surface of the inclusion (green and blue colour can be found in the inclusion in (b) and (d), respectively).

In the colour-code map, the pressures show increased values obviously in the non-fracture inclusion with the maximum pressure of 8.1 kbar. Contrarily, the pressure of the leaked inclusion decreased to 2.4 kbar (Fig. 5.23). The concentration of the highest pressure was not at the rim of the inclusion as always seen in the medium heating temperature experiments. Several high pressure values were found at other positions of the inclusions instead. This process was caused by the melting and recrystallization of the m-ZrO_2 and the SiO_2-rich phase of the former zircon inclusion, formed at the high-temperature heat treatment. This forming of these phases yielded the increasing of the stress between them and the host corundum. This transformation of phases has been confirmed by the chemical analyse by the back-scattered electron image as described below.

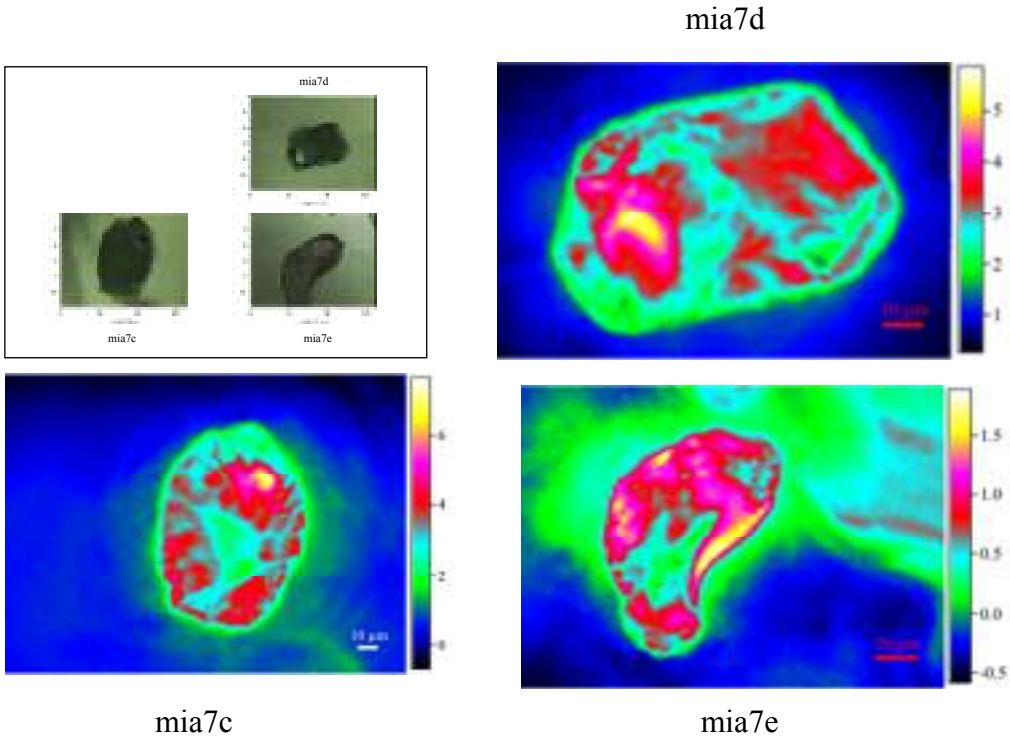

Fig. 5.23 Colour-code maps of the pressure of the heated zircon inclusion at 1800°C. The inset shows the original molten inclusion.

For the qualitative chemical analysis of the molten inclusion, another molten inclusion near the surface of corundum host was studied by Scanning Electron Microscope (SEM). The heated corundum sample was polished to expose the near-surface molten inclusion. To investigate the phase transformation and the composition, the back-scattered electron image of the SEM measurement with EDX-System was taken (Fig. 5.24). The image showed the unusually embayment features of the decomposing reaction. In this embayment, the zircon inclusion was entirely altered with no zircon surviving. There were two phases with high contrast in the image which are of bright colour displaying dendritic quenched crystals and material irregularly distributed with grey colour inside the dendritic area. The chemical contents were qualitatively measured in both areas. The analysed results of the bright area are clearly detectable as the ZrO_2 phase, which was also determined by Raman spectroscopy as baddeleyite (m-ZrO_2). The grey shaded material inside the dendritic intergrowth contained not only a phase composed of Al_2O_3-SiO_2, which can not be detected by Raman spectroscopy because of the low intensity of the Raman bands and / or the bad crystallinity, but also other elements such as Na, Ca, Mg, Fe, and Ti are found in this area which is a similar result as given by Wang et al. (2006). These other elements which can be found in this obviously SiO_2-rich phase were reported by Thomas (2003) who stated these elements to be decomposed from the molten inclusion inside the former zircon inclusion. Finally, it can be concluded that the zircon inclusion transformed totally into m-ZrO_2 and SiO_2-rich phase after being heated at 1800°C confirming with the conclusion of Budinikov and Litvakovski (1956) that the eutectic temperature of Al_2O_3-ZrO_2-SiO_2 system should be at around 1700°C - 1800°C (Fig. 5.25). Therefore, the host corundum has be reacted with the inclusion at 1800°C and Al_2O_3 can be found as a component included in the SiO_2-rich phase (grey shade in Fig. 5.24).

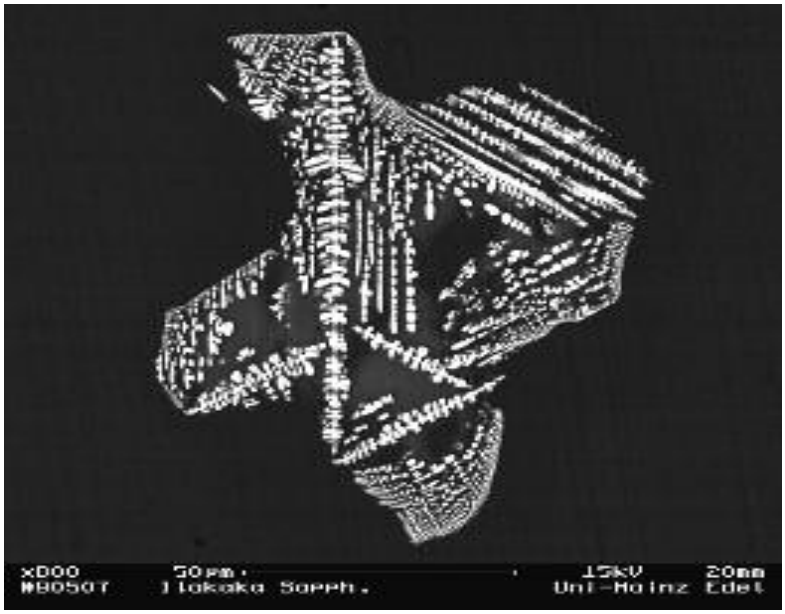

Fig. 5.24 Back-scattered electron image of dendritic quenched crystals of m-ZrO_2 (baddeleyite) in the white colour and the SiO_2-rich phase including with Na, Ca, Mg, Fe, and Ti composition inside the dendritic area.

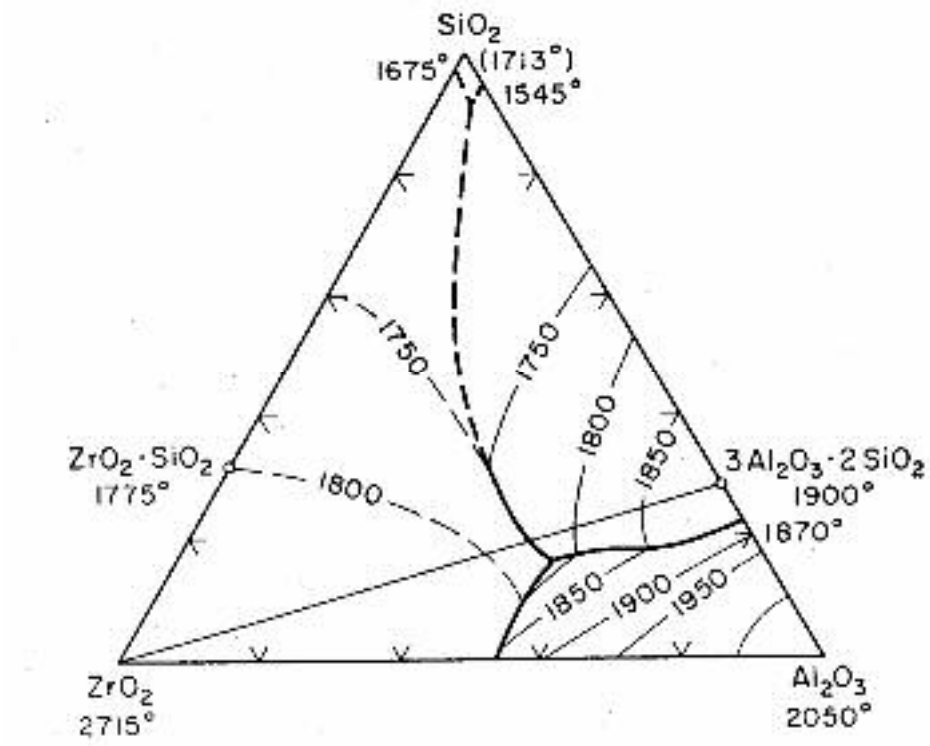

Fig. 5.25 Phase diagram of Al_2O_3–SiO_2–ZrO_2 showing the eutectic forming temperature (Budnikov and Litvakovskii, 1956).

6. Further study

In case of determining the original pressure trapped during crystal growth of the host corundum, the conditions for the trapped pressure around the inclusion should be that for a single mineral phase, no phase transition, no deformation of the inclusion, and the elastically deformation taking place only during tectonic transportation. The side effect of the transportation of the host to the earth's surface impacts the differential expansion, affecting the pressure relation between the inclusion and the host. This phenomenon can also be found in the zircon inclusion and the corundum host in this study where both minerals have different thermal expansion coefficients. The coefficient value of zircon is lower than that of corundum, 3.2 - 4.5 x 10^{-6}/°C for zircon (Bayer, 1972) and 7.6 x 10^{-6}/°C for corundum (White and Roberts, 1983). Therefore, the volume of the corundum host, including the zircon inclusion, decreases more than the volume of the inclusion itself during the temperature decrease and the change of pressure during the process of transportation. Concerning the elastic moduli of natural zircon crystals it was reported by Özkan (1976) that the elastic constant of natural zircon is extremely sensitive to the degree of crystalline damage and can decrease by non-spherical defect clusters, microcracks, and pores, generated during the radiation damage. Additionally, Harley and Kelly (2007) reported that the volume expansion of zircon is around 0.6% from room temperature to its stability limit of 1690°C. The trapped pressure between the zircon inclusion and the corundum host is the combination of the original internal pressure at the earth's surface and the pressure of the expansion volume by the metamictization activity. In this study, therefore, the original trapped pressure of the zircon inclusion and its host from Ilakaka can not be determined because they are radiation-damaged zircons.

A further study is in progress to determine the original trapped pressure between the crystalline-zircon inclusion and its host by this Cr^{3+} fluorescence technique and also with the other mineral inclusion in the corundum host.

7. Conclusions

7.1 Hydroxide minerals inclusions

The core sample of translucent ruby and the powder of hydroxyl minerals as diaspore, boehmite, gibbsite and bayerite were studied by NETZSCH STA 429 CD (Simultaneous thermogravimetry–differential scanning calorimetry) to determine the temperature of decomposition of aluminium hydroxyl minerals which are included in ruby samples. They were heated up to 1200 °C comparing the reactions with the standard sample (powder of α-Al_2O_3) based on the TG and DTA methods.

The results of TG show the clear separation of the two structures of hydroxyl groups which have lost the weight at different temperatures. The ruby sample showed the beginning temperature of the weight loss closely to the diaspore and/or the boehmite dehydration temperature at around 480°C and the ending of the reaction at around 600°C. The curve could be explained with diaspore alone, boehmite or the combination pattern of the both hydroxide minerals.

The results of DTA showed the endothermic process in every mineral. With the endothermic peaks, they can be divided into two groups which are similarly to the groups found by the TG. The ruby sample showed the same pattern as for diaspore and/or boehmite.

From both results, it can be concluded that the included hydroxyl minerals in the translucent ruby sample were diaspore and/or boehmite. With this result, diaspore and boehmite should not be found in heat treated corundum crystals that have been heated at temperatures over 600°C.

7.2 Radiation-damaged zircon inclusions

Under microscopic observation, the surface alteration of zircon inclusions in corundum can be observed at temperatures between 1400°C and 1600°C (according to Wang, et al., 2006: 1450 °C). The surface characteristics change detectably from transparent into frosted-like. Then, between 1600°C and 1800 °C, the inclusion melts.

With Raman spectroscopy, the minimum width of FWHM of the zircon inclusions in unheated Ilakakan corundums is approximately 5.4 cm^{-1}, which indicates that the inclusions are radiation-damaged zircons. On the other hand, the FWHM of the zircon inclusions heated at more than 1000°C is lower than 4 cm^{-1}, which is close to the value of the crystalline zircon. Thus, Raman spectroscopy can be used to determine Ilakakan corundum, which has been heated at more than 1000°C.

Normally, a radiation-damaged zircon shows the Raman shift to lower values, compared with a crystalline zircon. But the zircon inclusions in the unheated Ilakakan corundums show the Raman shift to higher values than the crystalline zircons. The lowering Raman shift in the radiation-damaged zircon is due to the disordered lattice structure of the radiation-damaged zircon. Contrary, the shift to higher Raman values in the zircon inclusion is caused by the following reasons:

1.) The high pressure around the inclusion of round about 5 kbar
2.) The stress in the zircon inclusion, produced by the expansion of the radiation-damaged zircon inclusion compared with the untreated zircon.
3.) The stress which increases due to the fast cooling rate after heat treatment process.
4.) The expansion of the decomposed minerals, baddeleyite (m-ZrO_2) and SiO_2-rich phase substituting the zircon inclusion after the high-temperature heat treatment.

The crystallinity of zircon inclusions in Ilakaka corundums is an obvious indicator of a medium-temperature heat treatment. At 500 °C, a slight shift of the Raman position and the insignificant changes of FWHM values can already be observed. Heated at 800 °C, the zircon inclusions of Ilakakan corundums show the results of lower Raman position and narrower FWHM values of the ν_3 band in comparison with the unheated ones. After treated with heat at 1,000 °C, it can be noticeably seen that Raman positions and FWHM values of these zircon inclusions are completely different from those of all the unheated. With the FWHM value at this temperature, it can be concluded that the radiation-damaged zircon inclusion can entirely recrystallize after being annealed at 1000°C. This result is confirmed by the contraction of the zircon inclusion after recrystallization, which is indicated by the decreasing of the trapped pressure around the zircon inclusion. Moreover, the lower Raman shift of the ν_3 Raman band after annealing also supports the decreasing of the stress of the zircon inclusion.

From 1200°C, the FWHM of the band remains unchanged with the negligibly tiny decrease, while the Raman position increases continuously. This phenomenon can be explained by the decomposition of zircon to the monoclinic ZrO_2 (m-ZrO_2) and a SiO_2-rich phase. This phase change (from $ZrSiO_4$ to m-ZrO_2 and a SiO_2-rich phase) begins at the tiny rim of the zircon inclusion at around 1200°C, which is not detectable with the Raman spectroscopy. But the volume enlargement of the inclusion causes to increase the internal pressure and shear stress around the zircon inclusion which can be detected by the R_1 luminescence shift method. The higher Raman shift is influenced after being heated at 1400°C when the progressive decomposition at the rim affects the stress of the zircon inclusion. At 1600°C, the decomposition becomes plainly detected. Another or an additional explanation for the increasing pressure around and the shift to higher wavenumbers in the temperature range between 1200°C and 1400°C could be the increasing cooling rate with increasing temperature. This could introduce an additional

stress around the inclusion. All of the zircon inclusions in this study melt during heat treatment at 1800°C. The inclusions transform into two solid phases, m-ZrO_2 (baddelyite-like) and SiO_2-rich phase. The maximum stress between the zircon inclusion and the corundum host develops close to the m-ZrO_2 and SiO_2-rich phase, with the maximum pressure at 8.1 kbar.

However, these results, especially the determination of the lower FWHM values in the unheated samples, need more statistic investigation and more variations of annealing experiment conditions, such as the temperature and the duration of heating, in order to attain more comprehensive results.

8. References

_____, 2002. Raman products technical note: Confocal Raman microscopy, RamanRxn Systems, *Kaiser Optical Systems, Inc*. No. 1350.

_____, 2006. Standardised gemmological repost wording, information sheet #4. *Laboratory Manual Harmonisation Committee (LMHC)*.

_____, 2007. Tanabe-Sugano diagram. The Pennsylvania State University. Available from: http://chemistry.bd.psu.edu/jircitano/TSdiagram.pdf (Accessed 10October 2007)

Baldwin, K.J. & Batchelder, D.N., 2001. Confocal Raman microspectroscopy through a planar interface. *Applied Spectroscopy*, **55**, 517-524.

Barnett, J.D., Block, S. and Piermarini, G.J., 1973. An optical fluorescence system for quantitative pressure measurement in the Diamond-Anvil Cell. *The Review of Scientific Instruments*, 44 (1), 1-9.

Barron, L.M., 2003. A simple model for the pressure preservation index of inclusions in diamond. *American Mineralogist*, 88, 1615-1619.

Bayer, G., 1972. Thermal expansion of ABO_4-compounds with zircon- and scheelite structures. *Journal of the Less-Common metals*, 26 (2), 255-262.

Berry, L.G., Mason, B., and Dietrich, R.V., 1983. *Mineralogy*, 2nd edition: Concepts, Descriptions and Determinations. W.H. Freeman and Company, San Francisco.

Broersma, A., Bruyn, P.L.de, Geus, J.W., and Stol, R.J., 1978. Simultaneous DTA and DTG measurements on aluminium oxide monohydroxides. *Journal of Thermal Analysis*, 13, 341-355.

Budinikov, P.P. and Litvakovski, A.A., 1956. (Title unknown). *Doklady Akademia Nauk S.S.S.R.*, Vol. 106, 268.

Capitani, G.C., Leroux, H., Doukhan, J.C., Rios, S., Zhang, M., and Salje, E.K., 2000. A TEM investigation of natural metamict zircons: structure and recovery of amorphous domains. *Physsics and Chemistry of minerals*, 27, 545-556.

Carim A.H., Rohrer, G.S., Dando, N.R., Tzeng S.Y., Rohrer, C.L., and Perrotta, A.J., 1997. Conversion of diaspore to corundum: A new α-Alumina transformation sequence. *Journal of the American Ceramic Society*, 80 (10), 2677-80.

Carlone, C., 1992. Raman spectrum of zirconia-hafnia mixed crystals. *Physical Review B*, 45 (5), 2079-2084.

Chen, X.J., Struzhkin, V.V., King, S., Mao, H.K., and Hemley, R.J., 2004. Pressure-induced phonon frequency shifts in transition-metal nitrides. *Physical Review B*, 70, 014501-1-6.

Colombo, M., Chrosch, J., and Salje, E.K.H., 1999. Annealing metamict zircon: A powder X-ray diffraction study of a highly defective phase. *Journal of the American Ceramic Society*, 82 (10), 2711-2716.

Dawson, P., Hargreave, M.M., Wilkinson, G.R., 1971. The vibrational spectrum of zircon ($ZrSiO_4$). *Journal of Physics C: Solid State Physics*, 4, 240-256.

Deer, W.A., Howie, R.A., and Zussman, J., 1962. *Rock-forming minerals*. Vol. 5. Non-Silicate. Longman, London.

Di Rupo, E., Gilbart, E., Carruthers, T.G., and Brook, R.J., 1979. Reaction hot-pressing of zircon-alumina mixtures. *Journal of Materials Science*, 14, 705-711.

Heiman, D., 2007. *Spectroscopy of ruby fluorescence*. Advanced Physics Lab-1, Northeastern University.

Eggert, J.H., Goettel, K.A., and Silvera, I.,F., 1989a. Ruby at high pressure. I. Optical line shifts to 156 GPa. *Physical Review B*, 40 (8), 5724-5732.

Eggert, J.H., Goettel, K.A., and Silvera, I.,F., 1989b. Ruby at high pressure. II. Fluorescence lifetime of the R line to 130 GPa. *Physical Review B*, 40 (8), 5733-5738.

Eggert, J.H., Moshary, F., Evans, W.J., Goettel, K.A., and Silvera, I.,F., 1989c. Ruby at high pressure. III. A pumping scheme for the R lines up to 230 GPa. *Physical Review B*, 44 (14), 7202-7208.

Ervin, G. Jr., 1952. Structural interpretation of the diaspore-corundum and boehmite-γ-Al_2O_3 transitions. *Acta Crystallophica*, 5, 103-108.

Everall, N., 2004a. Depth profiling with confocal Raman microscopy, Part I. *Spectroscopy*, 19 (10), 22-27.

Everall, N., 2004b. Depth profiling with confocal Raman microscopy, Part II. *Spectroscopy*, 19 (11), 16-25.

Ewing, R.C., 1999. Nuclear waste forms for actinides. *Proceeding of the National Academy of Sciences of the United States of America*, 96 (7), 3432-3439.

Fei, Y., 1995. *Thermal expansion. Mineral physics and crystallography; A Handbook of physical constants*. The American Geophysical Union.

Finger, L. and King, H., 1978. A revised method of operation of the single-crystal diamond cell and refinement of the structure of NaCl at 32 kbar. *American Mineralogist*, 63, 337-342.

Gaft, M., Reisfeld, R., and Panczer, G., 2005. *Luminescence spectroscopy of minerals and materials*. Springer.

Geisler, T., 2002. Isothermal annealing of partially metamict zircon: evidence for a three-stage recovery process. *Physics and Chemistry of Minerals*, 29, 420-429.

Geisler, T. and Pidgeon, R.T., 2002. Raman scattering from metamict zircon: comments on "Metamictisation of natural zircon: accumulation versus thermal annealing of radioactivity-induced damage" by Nasdala et al., 2001. *Contribution to Mineralogy and Petrology*, 143, 750-755.

Gentry, R. V., 1974. Radiation halow in a radiochronological and cosmological perspective. *Science*, 84, 62-66.

Giese Jr, R.F., 1976. Hydroxyl orientations in gibbsite and bayerite. *Acta Crystallographica B*, 32, 1719-1723.

Giuliani, G., Dubessy, J., Banks, D., Vinh, H.Q., Lhomme, T., Pironon, J., Garnier, V., Trinh, P.T., Long, P.V., Ohnenstetter, D., And Schwarz, D., 2003. CO_2-H_2S-COS-S_8-AlO(OH)- bearing fluid inclusions in ruby from marble-hosted deposits in Luc Yen area, North Vietnam. *Chemical Geology*, 194. 167-185.

Giuliani, G., Fallick, A., Rakotondrazafy, M., Ohnenstetter, D., Rakotosamizanany, S., Razanatseheno, M., Offant, Y., Garnier, V., Dunaigre, C., Schwarz, D., Mercier, A., Ratrimo, V., and Ralison, B., 2007. Oxygen isotope systematics of gem corundum deposits in Madagascar: relevance for their geological origin. *Miner Deposita*, Vol. 42, 251-270.

Glinnemann, J., Kusaka, K., and Harris, J.W., 2003. Oriented graphite single-crystal inclusions in diamond. *Zeitschrift für Kristallographie*, 218, 733-739.

Grimsditch, M.H., Anastassakis, E. & Cardona, M. (1978): Effect of uniaxial stress on the zone-center optical phonon of diamond. *Physical Review B*, **18**, 901-904.

Groß, M., Kolarik, V., Singheiser, L., Engel, W., and Eisenreich, N., Temperature resolved evaluation of residual stresses in an α-Al2O3 scale using parallel beam X-ray diffraction. *The proceedings of the Denver X-ray conference; Advances in X-ray Analysis*, Vol. 42, 451-459.

Gübelin, E.J., 1973. Internal world of gemstones. *ABC Verlag, Zürich*, reprinted 1983.

Gübelin, E.J. and Koivula, J.I., 1986. Bildatlas der Einschlüsse Edelsteinen. *ABC Verlag, Zürich.* 532.

Guo, J., O´Reilly, S.Y., and Griffin, W.L., 1996. Zircon inclusions in corundum megacrysts: I. Trace element geochemistry and clues to the origin of corundum megacrysts in alkali basalts. *Geochimica et Cosmochimica Acta*, Vol. 60 (13), 2347-2363.

Hänni, H.A. (1982): Zur Erkennung diffusionsbehandelter Korunde. *Zeitschrift der Deutschen Gemmologischen Gesellschaft*, **31**, 49-57.

Gupta, Y.M. and Shen, X.A., 1991. Potential use of the ruby R2 line shift for static high-pressure calibration. *Applied Physics letters*, 58 (6), 583-585.

Häger, T., and Dzung, P. T., 2003. Quantitative laser-induced photoluminescence and cathodoluminescence spectrosscopy of natural and synthetic rubies. *Geo- and Material-Science on Gem-Minerals of Vietnam. Proceeding of the International Workshop, Hanoi, October 01-08*, 122-128.

Harley, S.L. and Kelly, N.M., 2007. Zircon: Tiny but timely. *Elements*. 3 (1), 13-18.

Hazen , R.M. and Finger, L.W., 1979. Crystal structure and compressibility of zircon at high pressure. *American Mineralogist*, 64, 196-201.

He, J., and Clarke, D. R., 1997. Polarization dependence of the Cr^{3+} R-line fluorescence from sapphire and its application to crystal orientation and piezospectroscopic measurement. *Journal of the American Ceramic Society*, 80, Issue 1, pp. 69.

Heaman, L.M., Bowins, R., and Crocket, J., 1990. The chemical composition of igneous zircon suites: Implications for geochemical tracer studies. *Geochemica et Cosmochimica Acta*, Vol. 54, 1597-1607.

Horn, P.D. and Gupta, Y.M., 1989. Luminescence R-line spectrum of ruby crystals shocked to 125 kbar along the crystal c axis. *Physical Review B*, 39 (2), 973-979.

Hoskin, P.W.O. and Rodgers, K.A., 1996. Raman spectral shift in the isomorphous series $(Zr_{1-x}Hf_x)$ SiO_4. *European Journal of Solid State Inorganic Chemistry*, 33, 1111-1121.

Howard, C.J., Hill, R.J., and Reichert, B.E., 1988. Structures of the ZrO_2 polymorphs at room temperature by high-resolution neutron powder diffraction. *Acta Crystallographica Section B*, 44, 116-120.

Hughes, R. W., 1997.*Ruby and sapphire*. RWH Publishing. Colorado.

Izraeli, E.S., Harris, J.W., and Navon, O., 1999. Raman barometry of diamond formation. *Earth and Planetary Science Letters*, 173, 351-360.

Jayaraman, A., 1983. Diamond anvil cell and high-pressure physical investigations. *Reviews of Modern Physics*, 55 (1), 65-108.

Jovanic, B.R., 1997. Shift under pressure of the luminescence transitions of corundum doped with Mn^{4+}. *Journal of luminescence*, 75. pp. 171-174.
Klein, C. and Hurlbut, Jr, C., S., 1977. *Manual of Mineralogy*. John Wiley & Sons, INC. New York.

Knittle, E. and Williams, Q., 1993. High-pressure Raman spectroscopy of $ZrSiO_4$: Observation of the zircon to scheelite transition at 300 K. *American Mineralogist*, 78, 245-252.

Kolesov, B.A., Geiger, C.A., Armbruster, T., 2001. The dynamic properties of zircon studied by single-crystal X-ray diffraction and Raman spectroscopy. *European Journal of Mineralogy*, 13, pp. 939-948.

Lam, P.K., Yu, R., and Lee, M.W., 1990. Structural distortions and vibrational modes in Mg_2SiO_4. *American Mineralogist*, Vol. 75, 109-119.

Levin, E.M., Robbins, C.R., and McMurdie, H.F., 1964. *Phase diagrams for ceramists*. The American Ceramic Society, Inc.

Liu, H., Lim, K. S., Jia, W., Strauss, E., and Yen W. M., 1988. Effects of tensile stress on the R lines of Cr^{3+} in a sapphire fiber. *Optical Letters*, 13 (10), 931-933.

Liu, L.G., Mernagh, T.P., and Jaques, A.L., 1990. A mineralogical Raman spectroscopy study on eclogitic garnet inclusions in diamonds from Argyle. *Contributions to Mineralogy and Petrology*, 105, 156-161.

Malinowski, M., 1987. A Diamond-anvil high-pressure cell for X-ray diffraction on a single crystal. *Journal of Applied Crystallography*, 20, 379-382.

Mao, H. K., Xu, J., and Bell, P. M., 1986. Calibration of the ruby pressure gauge to 800 kbar under quasihydrostatic conditions, *Journal of Geophysical Research*, 91 (B5), pp.4673-4676.

McClure, S.F., Smith, C.P., Wang, W., and Hall, M., 2006. Identification and durability of lead glass-filled rubies. *Gems and Gemology*, 42 (1), 22-34.

McMillan, P.F. and Hofmeister, A.M., 1988. Infrared and Raman spectroscopy: Reviews in Mineralogy: Spectroscopic methods in mineralogy and geology; Hawthorne, F.C. eds. *Mineralogical Society of America*, Vol. 18, 99-150.

Milisenda, C.C., Henn, U. & Henn, J. (2001): New gemstone occurrences in the south-west of Madagascar. – *Journal of Gemmology*, **27,** 385-394.

Milisenda, C.C.,Horikawa, Y., and Henn, U., 2005. Rubin mit bleihaltigen Gläsern Gefüllt. *Zeitschrift der Deutschen Gemmologischen Gesellschaft*, 54, 35-42.

Mitra, S.S., Brafman, O., Daniels, W.E., and Crawford, R.K., 1969. Pressure-induced phonon frequency shifts measured by Raman scattering. *Physical Review B*, 186 (3), 942-944.

Munro, R.G., Piermarini, G.J., and Block, S., 1985. Model line-shape analysis for the ruby R lines used for pressure measurement. *Journal of Applied Physics*, 57 (2), 165-169).

Murakami, T., Chakoumakos, B.C., Ewing, R.C., Lumpkin, G.R., and Weber, W.J., 1991. Alpha-decay event damage in zircon. *American Mineralogist*, 76, 1510-1532.

Nasdala, L., Brenker, F.E., Glinnemann, J., Hofmeister, W., Gasparik, T., Harris, J.W., Stachel, T., & Reese, I. 2003. Spectroscopic 2D-tomography: Residual pressure and strain around mineral inclusions in diamonds. *European Journal of Mineralogy*, 15, 931-935.

Nasdala, L., Götze, J., Hanchar, J.M., Gaft, M., and Krbetschek, M., 2004. Luminescence techniques in Earth Sciences. *EMU Notes in Mineralogy*, 6, 43-91.

Nasdala, L, Hanchar, J. M., kronz, A., and Whitehouse, M.J., 2005. Long-term stability of alpha particle damage in natural zircon. *Chemical Geology*, 220, 83-103.

Nasdala, L., Hofmeister, W., Harris, J.W., and Glinnemann, J., 2005. Growth zoning and strain patterns inside diamond crystals as revealed by Raman maps. *American Mineralogist*, 90, 745-748.

Nasdala, L., Irmer G., and Raymond J., 2002b. Radiation damage ages: Practical concept or impractical vision? – Reply to two comments on "Metamictisation of natural zircon: Accumulation versus thermal annealing of radioactivity-induced damage" and further discussion. *Contributions to Mineralogy and Petrology*, 143, 758-765.

Nasdala, L., Irmer, G., and Wolf, D., 1995. The degree of metamictization in zircon: a Raman spectroscopic study. *European Journal of Mineralogy*, 7, 471-478.

Nasdala, L., Lengauer C. L., Hanchar J. M., Kronz A., Wirth R., Blanc P., Kennedy A. K., and Seydoux-Guillaume A-M., 2002a. Annealing radiation damage and the recovery of cathodoluminescence. *Chemical Geology*, 191, 121-140.

Nasdala, L., Pidgeon, R.T., and Wolf, D., 1996. Heterogeneous metamictization of zircon on a microscale. *Geochimica et Cosmochimica Acta*, 60 (6), 1091-1097.

Nasdala, L., Wenzel M., Vavra G., Irmer G., Wenzel T., and Kober B., 2001. Metamictisation of natural zircon: accumulation versus thermal annealing of radioactivity-induced damage. *Contributions to Mineralogy and Petrology*, 141, 125-144.

Nasdala, L., Zhang M., Kempe U., Panczer G., Gaft M., Andrut M., and Plotze M., 2003. Reviews in Mineralogy and Geochemistry (John M. Hanchar & Paul W.O. Hoskin, editors), Spectroscopic methods applied to zircon. *Mineralogical Society of America*, 53. pp. 427-467.

Nelson, D. F., and Sturge, M. D., 1965. Relation between absorption and emission in the region of the R lines of ruby. *Physical review*, 137 (4a), 1117-1130.

Özkan, H. (1976): Effect of nuclear radiation on the elastic moduli of zircon. *Journal of Applied Physics*, 47, 4772-4779.

Patra, A., Tallman, R.E., and Weinstein, B.A., 2005. Effect of crystal structure and dopant concentration on the luminescence of Cr^{3+} in Al_2O_3 nanocrystals. *Optical Materials*, Vol. 27, 1396-1401.

Piermarini, G.J., 2001. High pressure X-Ray crystallography with the diamond cell at NIST/NBS. *Journal of Research of the National Institute of Standards and Technology*, 106 (6), 889-920.

Piermarini, G.J., Block, S., Barnett, J.D., and Forman, R.A., 1975. Calibration of the pressure dependence of the R1 ruby fluorescence line to 195 kbar. *Journal of Applied Physics*, 46 (6), 2774-2780.

Powell, R. C., Dibartolo, B., Birang, B., and Naiman, C. S. 1967. Fluorescence studies of energy transfer between single and pair Cr^{3+} systems in Al_2O_3. *Physical Review*, 155 (2), 296-308.

Ragan, D. D., Gustavsen, R., and Schiferl, D., 1992. Calibration of the ruby R1 and R2 Fluorescence shifts as a function of temperature from 0 to 600 K. *Journal of Applied Physics*, 72 (12), 5539-5544.

Rankin, A.H. and Edwards, W., 2003. Some effects of extreme heat treatment on zircon inclusions in corundum. *Journal of Gemmology*, 28(5), 257-264.

Rio, S. and Boffa-Ballaran, T., 2003. Microstructure of radiation-damaged zircon under pressure. *Journal of Applied Crystallography*, 36, 1006-1012.

Ruan, H.D., Frost, R.L., and Kloprogge, T., 2001. Comparison of Raman spectra in characterizing gibbsite, bayerite, diaspore and boehmite. *Jounal of Raman Spectroscopy*, 32, 745-750.

Sakkaravej, S., Sutthirat C., Pisutha-Arnond V., Wanthanakul, P., Pumpeng, S., and Haeger, T., 2005. Characteristics and thermal treatment of blue shade sapphires from Ilakaka-Sakaraha deposits, Madagascar. *"Gem-Materials and Modern Analytical Methods" Proceedings of the International Symposium, Hanoi, September 26 – October 2, 2005*, 255-262.

Schmetzer, K., Bosshard, G. & Hänni, H.A. (1982): Naturfarbene und behandelte gelbe und orange-braune Saphire. *Zeitschrift der Deutschen Gemmologischen Gesellschaft*, 31, 265-279.

Schmetzer, K. and Medenbach, O., 1988. Examination of three-phase inclusions in colorless, yellow, and blue sapphires from Sri Lanka. *Gems and Gemology*. Summer, 107-111.

Schmidt, C. and Ziemann, M.A., 2000. In-situ Raman spectroscopy of quartz: A pressure sensor for hydrothermal diamond-anvil cell experiments at elevated temperatures. *American Mineralogist*, 85, 1725-1734.

Shannon, R.D., 1976. Revised effective ionic radii and systematic studies of interatomic distances in halides and chalcogenides. Acta *Crystallographica A*, Vol. 32, 751-767.

Sharma, S. and Fupta, Y.M., 1991. Theoretical analysis of R-line shifts of ruby subjected to different deformation conditions. *Physical Review B*, Vol. 43 (1), 879-893.

Shen, X.A. and Gupta, Y.M., 1993. Effect of crystal orientation on ruby R-line shifts under shock compression and tension. *Physical Review B*, 48 (5), 2929-2940.

Sobolev, N.V., Fursenko, B.A., Goryainov, S.V., Shu, J., Hemley, R.J., Mao, H.K., and Boyd, F.R., 2000. Fossilized high pressure from the Earth´s deep interior: The coesite-in-diamond barometer. *Proceedings of the National Academy of Sciences of the United States of America*, 97 (2), 11875-11879.

Subbarao,E.C., Agrawal, D.K., Mckinstry, H.A., Sallese, C.W. and Roy, R., 1990. Thermal expansion of compounds of zircon structure. *Journal of American Ceramics Society*, 73 (5), 1246-52.

Sutherland,F.L., Hoskin, P.W.O:, Fanning, C.M., and Coenraads, R.R., 1998. Models of corundum origin from alkali basaltic terrains: a reappraisal. *Contributions to Mineralogy and Petrology*, Vol. 133, 356-372.

Wunder, S.L. and Schoen, P.E., 1981. Pressure measurement at high temperatures in the diamond anvil cell. *Journal of Applied Physics*, 52, 3772-3775.

Tanabe, Y. and Sugano, S., 1954. On the absorption spectra of complex ions. I and II. *Journal of the Physical Society of Japan*, Vol. 9, 753-766; 766-779.

Tardieu, A., Cansell, F., and Petitet, J.P., 1990. Pressure and temperature dependence of the first-order Raman mode of diamond. *Journal of applied physics*, 68 (7), 3243-3245.

Temuujin, J., Jadambaa, Ts., Mackenzie, K.J.D., Angerer, P., Porte, F., and Riley, F., 2000. Thermal formation of corundum from aluminium hydroxides prepared from various aluminium salts. *Bulletin of Materials Science*, 23 (4), 301-304.

Thomas, B.J., 2003. Melt inclusion geochemistry. Dissertation, *Faculty of the Virginia Polytechnic Institute and State University*.

Trachenko, K., Dove, M.T., and Salje, E.K.H., 2002. Structural changes in zircon under alpha decay irradiation. *Physical Review B*, 65, (180102), 1-3.

Wang, S.X., Begg, B.D., Wang, L.M., Ewing, R.C., Weber, W.J., and Govidan Kutty, K.V., 1999. Radiation stability of gadolinium zirconate: a waste form for plutonium disposition. *Journal of Material Research*, 14, 4470-4473.

Wang, W., Scarratt, K, Emmett, J.L., Breeding, C.M., and Douthit, T.R., 2006. The effects of heat treatment on zircon inclusions in Madagascar sapphires. *Gems and Gemology*, 42 (2), 134-150.

Wang, S.Y., Shama, S.K., and Cooney, T.F., 1993. Micro-Raman and infrared spectral study of forsterite under pressure. *American Mineralogist*, 78, 469-476.

Wanthanachaisaeng, B. and Häger, T., 2006a. Abstract: Pressure-mapping around inclusions in corundum crystals determined by the shift of Cr^{3+} luminescence bands. *AOGS 3rd Annual Meeting*.

Wanthanachaisaeng, B. and Häger, T., 2006b. Pressure determination around metamict zircon inclusions in corundum and their behavior on heat treatment; *The 1st GIT International Gem &Jewelry Conference (GIT 2006)*.

Wanthanachaisaeng, B. and Häger, T., 2006c. Raman Spectroscopic Study of Metamict Zircon Inclusions in Corundum and Their Behaviour on Heat Treatment. *The 1st GIT International Gem &Jewelry Conference (GIT 2006)*.

Wanthanachaisaeng, B., Häger, T., and Hofmeister, W., 2005. Determination of pressure around inclusions in corundum crystals by the shift of Cr^{3+} luminescence bands. *Gem-Materials and Modern Analytical Methods: Proceedings of Internationsl Symposium, Hanoi, September 26 – October 2, 2005*, 125-134.

Wanthanachaisaeng, B., Häger, T., Hofmeister, W., and Nasdal, L., 2006d. Raman- und fluoreszenz-spexktroskopische Eigenschaften von Zirkon-Einschlüssen in chrom-haltigen Korundum aus Ilakaka und deren Veränderung durch Hitzebehandlung. *Zeitschrift der Deutschen Gemmologischen Gesellschaft*, 55, 119-132.

Wasiliewski, P.J., Senftle, F.E., Vaz, J.E., Thorpe, A.N., & Alexander, C.C., (1973): A study of the natural α-recoil damage in zircon by infrared spectra. *Radiation Effects*, **17**, 191-199.

Waychunas,G.A., 1988. Luminescence, X-Ray emission and new spectroscopies: Reviews in Mineralogy: Spectroscopic methods in mineralogy and geology; Hawthorne, F.C. eds. *Mineralogical Society of America*, Vol. 18, 639-694.

Wehrmeister, U. and Häger, T. (2006): *Edelsteine erkennen – Eigenschaften und Behandlung*. Rühle-Diebener-Verlag Stuttgart.

Westrenen, W.V., Frank, M.R., Fei, Y., Hanchar, J.H., Finch, R.J., and Zha, C.S., 2005. Compressibility and phase transition kinetics of lanthanide-doped zircon. Journal of the *American Ceramic Society*, 88 (5), 1345-1348.

White, G.K. and Roberts, R.B., 1983. Thermal expansion of reference materials: Tungsten and α-Al_2O_3. *High Temperatures-High Pressure*, 15, pp. 321-328.

Yen, J., and Nicol, M., 1992. Temperature dependence of the ruby luminescence method for measuring high pressures. *Journal of Applied Physics*, 72, Issue 12, pp. 5535-5538.

Yu, H. and Clarke, D.R., 2002. Effect of codoping on the R-line luminescence of Cr^{3+} -doped alumina. *Journal of the American Ceramic Society*, 85 (8), 1966-1970.

Zhang, Y., 1998. Mechanical and phase equilibria in inclusion-host systems. *Earth and Planetary Science Letters*, 157, pp. 209-222.

Zhang, M., Salje, E.K.H., Farnan, I., Graeme-Barber, A., Daniel, P., Ewing, R.C., Clark, A.M., and Leroux, H., 2000a. Metamictization of zircon: Raman spectroscopic study. *Journal of Physics: Condensed Matter*, 12, 1915-1925.

Zhang, M., Salje, E.K.H., Capitani, G.C., Leroux, H., Clark, A.M., Schlüter, J., and Ewing, R.C., 2000b. Annealing of α-decay damage in zircon: a Raman spectroscopy study. *Journal of Physics: Condensed Matter*, 12, 3131-3148.